

# RPWIA analysis of dynamical relativistic contributions in $^{16}\text{O}(\vec{e}, e'\vec{p})$ reactions

M.C. Martínez<sup>1</sup>, J.A. Caballero<sup>1</sup>, T.W. Donnelly<sup>2</sup>

<sup>1</sup>*Departamento de Física Atómica, Molecular y Nuclear  
Universidad de Sevilla, Apdo. 1065, E-41080 Sevilla, SPAIN*

<sup>2</sup>*Center for Theoretical Physics, Laboratory for Nuclear Science and Department of Physics  
Massachusetts Institute of Technology, Cambridge, MA 02139, USA*

---

## Abstract

Coincidence scattering of polarized electrons from nuclei with polarization transfer to outgoing nucleons is studied within the context of relativistic mean field theory. Effects introduced by the dynamical enhancement of the lower components of the bound nucleon wave function are analyzed for the polarized response functions and transferred polarization asymmetries assuming the relativistic plane-wave impulse approximation (RPWIA). Results obtained by projecting out the negative-energy components are compared with the fully-relativistic calculation for proton knockout from  $p_{1/2}$  and  $p_{3/2}$  shells in  $^{16}\text{O}$  for a variety of kinematic situations. The crucial role played by the relativistic dynamics in some spin-dependent observables is clearly manifested even for low/medium values of the missing momentum. The degree to which knowledge about nucleon form factors can be extracted from analyses of this type of process is also discussed.

*PACS:* 25.30.Rw, 14.20.Gk, 24.10.Jv, 24.30.Gd, 13.40.Gp *Keywords:* Nuclear reactions; Coincidence electron scattering; Polarized responses; Transferred polarization asymmetries; Positive- and negative-energy components; Nucleon form factors.

---

MIT/CTP#3215

# 1 Introduction

Over the years analyses of quasielastic coincidence electron scattering reactions have provided important insight into single-particle properties of nuclei, in particular, on the energies, momentum distributions and spectroscopic factors of nucleons in nuclei. Implicit in these analyses is the assumption that for quasielastic kinematics the reaction mechanism underlying  $(e, e'N)$  reactions can be treated with confidence in the impulse approximation (IA), i.e., assuming the virtual photon attaches to a single bound nucleon that absorbs the whole momentum ( $q$ ) and energy ( $\omega$ ), subsequently being ejected and detected (see [1, 2, 3] for details).

The simplest approach to studies of  $(e, e'N)$  reactions invokes the standard plane-wave impulse approximation (PWIA). There the  $(e, e'N)$  differential cross section factorizes into a ‘single-nucleon’ cross section describing the electron-nucleon scattering process, and a spectral function that gives the probability for finding a nucleon in the target nucleus with selected values of energy and momentum compatible with the kinematics of the process. This factorization property makes  $(e, e'N)$  reactions so appealing for investigations of nuclear structure, since it implies that single-particle distributions can in principle be probed in great detail.

Unfortunately, the PWIA is an oversimplified description of  $(e, e'N)$  processes. Firstly, distortion of both electron and nucleon wave functions due to electromagnetic and strong interactions with target and residual nuclei are necessary in order to perform detailed comparisons with experiment. Although these new ingredients in general destroy the factorization result, the interpretation of experimental data is still usually based on this property by defining an effective spectral function and an effective nucleon momentum distribution (or reduced cross section) that in PWIA corresponds exactly to the single-particle density in momentum space.

Secondly, the PWIA itself involves a non-relativistic truncation, and for years most theoretical work on  $(e, e'N)$  has been carried out on the basis of particular non-relativistic approximations [1, 3]. For instance, this is the case for the standard distorted-wave impulse approximation (DWIA) that is involved in performing comparisons with experiment which uses non-relativistic expressions for the nucleon current operator and wave functions. There, the current operator is evaluated by using a direct Pauli reduction involving expansions in powers of  $p/M_N$ ,  $q/M_N$  and  $\omega/M_N$ , where  $p$  is the missing momentum and  $M_N$  the nucleon mass, and the bound and scattered wave functions correspond to Schrödinger solutions with phenomenological non-relativistic potentials. Although DWIA has been satisfactorily used to describe  $(e, e'N)$  experiments performed during 1970 and 1980’s [1], its validity for the interpretation of experiments performed for the last decade where higher energies have become available is questionable. The values of the momenta and energies involved in these processes are high enough to invalidate the non-relativistic expansions assumed in DWIA and new relativistic analyses of  $(e, e'N)$  reactions become necessary.

A concerted effort has been made in recent years to incorporate relativity in the description of coincidence  $(e, e'N)$  processes [4, 5, 6, 7, 8]. Within the framework of the relativistic mean field approach, nuclear responses and differential cross sections for quasielastic coincidence electron scattering have been investigated [9, 10, 11, 12, 13]. In the relativistic

distorted-wave impulse approximation (RDWIA), bound and scattering wave functions are described by solutions of the Dirac equation with scalar and vector (S-V) potentials, and use is made of the relativistic free-nucleon current operator. By comparing standard DWIA and RDWIA calculations, relativistic contributions can then be cast into two general categories, kinematical and dynamical relativistic effects. The former are directly connected with the structure of the 4-vector current operator, compared with the non-relativistic one that usually involves  $p/M_N$ ,  $q/M_N$  and  $\omega/M_N$  expansions. In some studies [14, 15, 16], new ‘relativized’ current operators have been derived by making only expansions in  $p/M_N$ , but not in  $q/M_N$  or  $\omega/M_N$ . These new expressions retain important aspects of relativity not taken into account in the traditional non-relativistic approximation and in so-doing these should perhaps be called “semi-relativistic” approaches. The latter, dynamical relativistic effects, come from the difference between the relativistic and non-relativistic nucleon (bound and ejected) wave functions involved. Within these dynamical relativistic effects one may distinguish effects associated with the Darwin term (that mainly affects the determination of spectroscopic factors at low missing momenta) and effects due to the dynamical enhancement of the lower components of the relativistic wave functions (which are expected to be especially relevant at high missing momenta, although they have proven to play an important role for some particular observables even at low/medium  $p$  values). So far, fully-relativistic analyses of  $(e, e'p)$  reactions have clearly improved the comparison with experimental data. In [9, 10] it was shown that the non-local Darwin term causes an enhanced absorption when comparing RDWIA cross section with the DWIA one at moderate  $p$  values, thus predicting larger spectroscopic factors [9, 13]. For larger missing momenta the lower components of the relativistic wave functions start to play a more important role, enhancing the high momentum components of the nucleon wave functions. RDWIA calculations, compared with DWIA, produce larger cross sections at  $p > 300$  MeV/c, also improving agreement with experiment [11].

In parallel with such RDWIA calculations, we have also undertaken a more systematic study of the effects of the dynamical enhancement of the lower components within RPWIA, i.e., neglecting final-state interactions (FSI) between the outgoing nucleon and the residual nucleus. Although a description of FSI is necessary to analyze experimental data in detail, the RPWIA approach allows one to simplify the analysis of the relativistic effects, disentangling them from other distortion effects. Moreover, within RPWIA it is possible to get analytical expressions that explicitly incorporate the contributions in the various observables coming from the negative-energy components of the bound nucleon wave function. This subject was thoroughly developed in [17] (see also [18]) for the case of unpolarized  $A(e, e'N)B$  reactions. Nuclear response functions and cross sections were evaluated and compared with the standard PWIA-predictions. The effects introduced by the presence of negative-energy components in the relativistic bound nucleon wave function were shown to be very important for some observables even at low/moderate values of the missing momentum. In particular, the interference  $TL$  and  $TT$  responses were shown to be the most sensitive observables to dynamical effects of relativity affecting the lower components. These results have been shown also to persist in modeling where FSI are included. In fact, data obtained on  $R^{TL}$  and the left-right asymmetry  $A_{TL}$  provide a strong indication of the crucial role played by dynamical relativistic effects in  $(e, e'p)$  reactions [12, 13].

The main aim of this paper is to analyze whether these dynamical relativistic effects may also have a significant impact on the polarization observables. Since spin and relativity go hand in hand, one may *a priori* consider the relativistic approach to be better suited to describe nucleon polarization observables. As is well known, when polarization degrees of freedom are involved, a much richer variety of observables becomes accessible. These contain in general interferences between various amplitudes and consequently a complete decomposition into the electromagnetic matrix elements can in principle be achieved [19]. In this work we focus on the case of final-state nucleon polarization measurements, i.e.,  $A(\vec{e}, e'\vec{N})B$  processes, and we work within the context of the RPWIA. The analysis of polarized observables including final-state interactions within RDWIA will be presented in a forthcoming publication. Thus, this work follows closely the formalism presented in [17] for the unpolarized responses.

In recent years a number of experiments have been proposed or carried out to measure the polarization of the ejected nucleon in  $(\vec{e}, e'\vec{p})$  reactions [20, 21]. Specifically, a concerted experimental effort has been made with the aim of shedding some light on the issue of the form factors of nucleons inside the nuclear medium. Indeed, recoil nucleon polarization observables may be well-suited to provide valuable information on the nucleon form factors [20]. Such studies present clear advantages compared with the usual Rosenbluth separation method, as they do not require one to vary the electron beam energy and/or the scattering angle, thus eliminating the systematic uncertainties that make it so difficult to extract the electric nucleon form factor  $G_E$  at high  $|Q^2|$  using the Rosenbluth method. Furthermore, recoil polarization calculations for low/medium missing momenta have also proven to be relatively insensitive to different ingredients in the description of the reaction mechanism, namely off-shell ambiguities and optical potentials used to describe FSI [7].

The first measurements of recoil nucleon polarization were performed at Bates [22, 23] and Mainz [24] analyzing  ${}^2H(\vec{e}, e'\vec{n})$  and  ${}^2H(\vec{e}, e'\vec{p})n$  reactions. From these experiments a first estimation of the neutron and proton form factors was given at several values of  $Q^2$ . Recently, high precision polarization transfer measurements on complex nuclei have been presented by Malov et al. in  ${}^{16}O(\vec{e}, e'\vec{p}){}^{15}N$  [20], and by Dieterich et al. in  ${}^4He(\vec{e}, e'\vec{p}){}^3H$  [21]. Although the general conclusions in these two last experiments are not free from ambiguities due to experimental uncertainties, the authors in [21] show that standard non-relativistic calculations are in clear disagreement with the experimental data. This result constitutes a strong indication of the necessity for a fully-relativistic calculation in order to describe the spin transfer observables. Moreover, it also agrees with the general analysis presented in the case of induced polarization measurements [25, 26, 27], where the fully RDWIA calculation clearly provides a better description of the experimental data when compared with the standard non-relativistic DWIA analysis.

In this paper we present a systematic study within RPWIA of the new response functions that enter in the description of  $A(\vec{e}, e'\vec{N})B$  processes. Following the arguments presented for the unpolarized case in [17], here we extend the analysis to the polarized situation and for the polarized responses attempt to identify clear signatures that arise from the dynamical relativistic effects coming from the negative-energy projections (NEP) of the relativistic bound nucleon wave function. Moreover, the role played by the NEP on the transferred polarization is also analyzed in detail. The work presented here is being undertaken in

concert with studies of related issues involving relativistic effects in coincidence electron scattering with active polarization degrees of freedom. To attempt to integrate all of the work into one manuscript would be far too unwieldy and hence we have found what we hope are natural division points to subdivide the presentations. In the light of this it is important to understand how the various studies interact with one another:

- In an accompanying paper [28] the focus is placed on **kinematical** relativistic effects for responses and polarization observables, however strictly within the context of the PWIA. Both off-shell and ‘on-shell’ approaches are taken. Basic essential formalism is also collected and presented in that paper.
- In contrast in the present work we have emphasized the roles played by **dynamical** relativistic effects which arise from non-trivial relativistic content in the nuclear wave functions. The present study has been limited to initial-state dynamical effects and thus the final state is still treated as a relativistic plane wave, the so-called RPWIA.
- In work in progress effects in the final state are also being incorporated through **relativistic FSI**, constituting the RDWIA. Upon completing this third phase of the overall study meaningful comparisons with measured observables can be attempted.

The paper is organized as follows: in Section 2 we describe  $A(\vec{e}, e'\vec{N})B$  reactions within the context of the relativistic plane-wave impulse approximation. Here a separation of the polarized response functions and cross section into positive- and negative-energy projections is made. In Section 3 we present and discuss the results obtained for various kinematic situations. The role of the negative-energy components and their influence on various choices of the current operator and/or gauge in the single-nucleon responses is presented in Section 3.1. The total polarized hadronic responses and transferred polarization asymmetries are discussed in Sections 3.2 and 3.3, respectively. Finally, in Section 4 we summarize our main conclusions.

## 2 Analysis of $A(\vec{e}, e'\vec{N})B$ reactions in the Relativistic Plane-Wave Impulse Approximation

In the  $(\vec{e}, e'\vec{N})$  process a longitudinally polarized electron with 4-momentum  $K = (\varepsilon, \mathbf{k})$  is scattered through an angle  $\theta_e$  to a 4-momentum  $K' = (\varepsilon', \mathbf{k}')$ . The hadronic variables are denoted by  $P_A^\mu = (M_A, \mathbf{0})$ ,  $P_N^\mu = (E_N, \mathbf{p}_N)$  and  $P_B^\mu = (E_B, \mathbf{p}_B)$  representing the 4-momenta of the target, outgoing nucleon and residual nucleus, respectively. The 4-momentum transfer is given by  $Q^\mu = K^\mu - K'^\mu = (\omega, \mathbf{q})$ . Within the impulse approach (IA), the virtual photon is absorbed by a single nucleon in the nucleus whose 4-momentum is  $P^\mu = P_N^\mu - Q^\mu = (E, \mathbf{p})$ . As usual, electrons are treated in the extreme relativistic limit (ERL), i.e.,  $\varepsilon = k$ ,  $\varepsilon' = k'$ .

The general formalism for coincidence electron scattering reactions with the electron beam polarized and with the outgoing nucleon’s polarization measured has been presented in detail in previous work [1, 4, 5, 19, 29] – in particular, as noted above, the present work has been undertaken in concert with a focused study of kinematic relativistic effects in  $(\vec{e}, e'\vec{N})$

reactions [28] and the reader is directed to that accompanying paper for detailed discussions of our conventions. Here we restrict our attention to the Relativistic Plane-Wave Impulse Approximation (RPWIA) where the analysis of  $(\vec{e}, e'\vec{N})$  reactions is further simplified. In particular, the analyzing power  $A$  and induced polarization  $\mathbf{P}$  (see [4, 5] for details) are zero in that case, and only the transferred polarization asymmetry  $\mathbf{P}'$  survives. In terms of nuclear responses, from the total of eighteen response functions that enter in the general analysis of  $A(\vec{e}, e'\vec{N})B$  reactions [4, 5] only nine survive within RPWIA. Four ( $R_0^L$ ,  $R_0^T$ ,  $R_0^{TL}$  and  $R_0^{TT}$ ) represent the unpolarized responses and the five remaining ( $R_l^{T'}$ ,  $R_s^{T'}$ ,  $R_l^{TL'}$ ,  $R_s^{TL'}$  and  $R_n^{TL'}$ ) depend explicitly on the recoil nucleon polarization and only enter when the electron beam is also polarized. The polarized responses are referred to the coordinate system defined by the unit vectors  $(\mathbf{l}, \mathbf{s}, \mathbf{n})$  with<sup>1</sup>  $\mathbf{l}$  (parallel to the momentum  $\mathbf{p}_N$  of the outgoing nucleon),  $\mathbf{n}$  (perpendicular to the plane containing  $\mathbf{p}_N$  and the transfer momentum  $\mathbf{q}$ ), and  $\mathbf{s}$  (determined by  $\mathbf{n} \times \mathbf{l}$ ).

Although the plane-wave limit represents an oversimplified description of electron scattering reactions, our goal in this paper is not so much to compare the calculation with experimental data, for which FSI are surely necessary, but rather is to focus on the dynamical relativistic effects coming from the presence of negative-energy projections of the bound nucleon wave function, and to investigate how this enhancement of the lower components affects the recoil nucleon polarized responses. In this sense, the simplification of invoking the plane-wave limit may help us gain important insight when trying to disentangle effects of distortion from effects of high  $p$  components in the bound nucleon wave function and current operator. Moreover, the RPWIA cross section and response functions can be separated into contributions from positive- and negative-energy projections of the bound nucleon wave function. These contributions can be analyzed separately to yield a clear indication of how the factorization limit of the standard PWIA analysis breaks down.

The RPWIA formalism applied to the analysis of the unpolarized  $(e, e'N)$  reaction was developed in detail in [17]. Here we apply the same approach to the case of recoil nucleon polarization measurements, and hence simply summarize the basic ingredients needed to describe the new observables, referring the reader to [17] for further details. We use the conventions of [30].

The cross section is proportional to the contraction of the leptonic tensor  $\eta_{\mu\nu}$  with the hadronic tensor  $W^{\mu\nu}$  (see [28]):  $\eta_{\mu\nu}$  can be evaluated from the electron current matrix elements (see for instance [19]) and  $W^{\mu\nu}$  arises from bilinear combinations of the nuclear current matrix elements. Within RPWIA, requiring that the recoil nucleon polarization be measured, one can write for the latter

$$W^{\mu\nu} = \frac{2}{2j+1} \sum_m \left[ \bar{u}(\mathbf{p}_N, s_N) \hat{J}^\mu \Psi_\kappa^m(\mathbf{p}) \right]^* \left[ \bar{u}(\mathbf{p}_N, s_N) \hat{J}^\nu \Psi_\kappa^m(\mathbf{p}) \right], \quad (1)$$

where  $\Psi_\kappa^m(\mathbf{p})$  denotes the Fourier transform of the relativistic bound nucleon wave function  $\Psi_\kappa^m(\mathbf{r})$  which is a solution of the Dirac equation with S-V potentials. The indices  $\kappa$  and  $m$  denote the Dirac wave function quantum numbers (see Appendix A in [17] for details). An

---

<sup>1</sup>Here we use  $l$ ,  $n$  and  $s$  to label the three axes, whereas in [19] different conventions were adopted: there unprimed labels were reserved for initial-state polarizations and primed labels ( $l'$ ,  $n'$ ,  $s'$ ) were employed when final-state polarizations occur as here.

interacting relativistic wave function always presents a coupling to the free negative-energy Dirac spinors  $v$ . Letting  $\bar{E}$  denote the on-shell energy, i.e.,  $\bar{E} = \sqrt{p^2 + M_N^2}$ , this implies that the free relation between upper ( $u$ ) and lower ( $d$ ) components,

$$\frac{\boldsymbol{\sigma} \cdot \mathbf{p}}{\bar{E} + M_N} \phi^u = \phi^d, \quad (2)$$

does not hold in general for a bound relativistic wave function. This is what differentiates the RPWIA from the standard PWIA analysis. According to [17] (see also Appendix A) the nucleon current matrix elements can be split into two terms, one coming from the positive-energy projector involving the spinors  $u(\mathbf{p}, s)$ , and the other from the negative-energy projector involving the spinors  $v(\mathbf{p}, s)$ . At the level of the hadronic tensor the following decomposition results:

$$W^{\mu\nu} = W_P^{\mu\nu} + W_N^{\mu\nu} + W_C^{\mu\nu}, \quad (3)$$

where  $W_P^{\mu\nu}$  ( $W_N^{\mu\nu}$ ) is the contribution from positive- (negative-) energy projections only, while  $W_C^{\mu\nu}$  is a crossed term containing products of both positive- and negative-energy projections. Following the arguments developed originally in [17] and presented also for the case of recoil nucleon polarization in Appendix A, each of the contributions in Eq. (3) can be factorized into two terms, a single-nucleon tensor and a momentum distribution component,

$$W_P^{\mu\nu} = N_{uu}(p) \mathcal{W}^{\mu\nu} \quad (4)$$

$$W_N^{\mu\nu} = N_{vv}(p) \mathcal{Z}^{\mu\nu} \quad (5)$$

$$W_C^{\mu\nu} = N_{uv}(p) \mathcal{N}^{\mu\nu}. \quad (6)$$

Note, however, that the total tensor in Eq. (3) is a sum of three terms and does not in general factorize. Explicit expressions for the momentum distribution components  $N_{uu}(p)$ ,  $N_{vv}(p)$  and  $N_{uv}(p)$  in terms of the upper and lower components of the bound nucleon wave function are given in [17] and are also summarized in Appendix A. Let us recall that by imposing the free relation in Eq. (2), only the contribution  $N_{uu}(p)$  survives, i.e., all of the terms containing negative-energy projections become zero. In this limit factorization is recovered.

The single-nucleon tensors  $\mathcal{W}^{\mu\nu}$ ,  $\mathcal{Z}^{\mu\nu}$  and  $\mathcal{N}^{\mu\nu}$  are given by

$$\mathcal{W}^{\mu\nu} = \frac{1}{8M_N^2} \text{Tr} \left[ (\mathcal{P} + M_N) \bar{\mathcal{J}}^\mu (\mathcal{P}_N + M_N) (1 + \gamma_5 \not{\mathcal{S}}_N) \mathcal{J}^\nu \right] \quad (7)$$

$$\mathcal{Z}^{\mu\nu} = \frac{1}{8M_N^2} \text{Tr} \left[ (\mathcal{P} - M_N) \bar{\mathcal{J}}^\mu (\mathcal{P}_N + M_N) (1 + \gamma_5 \not{\mathcal{S}}_N) \mathcal{J}^\nu \right] \quad (8)$$

$$\mathcal{N}^{\mu\nu} = \frac{1}{8M_N^2} \text{Tr} \left[ \bar{\mathcal{J}}^\mu (\mathcal{P}_N + M_N) (1 + \gamma_5 \not{\mathcal{S}}_N) \mathcal{J}^\nu \gamma^0 \frac{\boldsymbol{\gamma} \cdot \mathbf{p}}{p} \not{\mathcal{P}} \right], \quad (9)$$

where we use the notation  $\bar{\mathcal{J}}^\mu \equiv \gamma_0 \mathcal{J}^{\mu+} \gamma_0$ .

The term  $\mathcal{W}^{\mu\nu}$  is the usual single-nucleon tensor appearing in standard PWIA for outgoing nucleon polarized scattering, while  $\mathcal{Z}^{\mu\nu}$  and  $\mathcal{N}^{\mu\nu}$  are new single-nucleon tensors that enter only when the bound nucleon wave functions contain non-zero negative-energy projections.

Note also that the three single-nucleon tensors in Eqs. (7-9) can be split into symmetric and antisymmetric terms. The symmetric terms do not depend on the recoil nucleon polarization and, when contracted with the symmetric part of the leptonic tensor which does not depend on the electron polarization, give rise to the four unpolarized responses  $R_0^L$ ,  $R_0^T$ ,  $R_0^{TL}$  and  $R_0^{TT}$  studied in detail in [17] (note that the unpolarized responses and single-nucleon tensors in [17] are twice the ones given here because of the spin projection operator included for the outgoing nucleon polarized situation; i.e., the factor of two is recovered upon performing “sum over final”). In contrast, the antisymmetric terms in Eqs. (7-9) depend linearly on the outgoing nucleon four-spin  $S_N^\mu$ . Their contractions with the antisymmetric part of the leptonic tensor, which contains the dependence on the incident electron polarization, give rise to the positive- and negative-energy contributions in the spin-dependent responses  $R_{l,s}^{T'}$  and  $R_{l,s,n}^{TL'}$ .

Next, let us recall that using the spin precession technique presented in [31], the non-diagonal spin single-nucleon tensor  $\mathcal{N}^{\mu\nu}$ , can be written in terms of a diagonal tensor constructed from spinors quantized with respect to a spin axis pointing along a generic direction,  $\mathcal{R}^{\mu\nu}(\theta_R, \phi_R)$ , as

$$\mathcal{N}^{\mu\nu} = \cos\theta \mathcal{R}^{\mu\nu}(0, 0) + \sin\theta \left( \cos\phi \mathcal{R}^{\mu\nu}\left(\frac{\pi}{2}, 0\right) + \sin\phi \mathcal{R}^{\mu\nu}\left(\frac{\pi}{2}, \frac{\pi}{2}\right) \right). \quad (10)$$

Here  $\theta$ ,  $\phi$  are the angles defining the direction of the bound nucleon momentum  $\mathbf{p}$  and the tensor  $\mathcal{R}^{\mu\nu}$  is given as

$$\mathcal{R}^{\mu\nu}(\theta_R, \phi_R) = \frac{1}{8M_N} \text{Tr} \left[ \mathcal{S}_L \bar{\mathcal{J}}^\mu (1 + \gamma_5 \mathcal{S}_N) (\not{p}_N + M) \mathcal{J}^\nu \right], \quad (11)$$

which is linear in the bound nucleon spin four-vector  $S_L^\mu$ ; its antisymmetric part also depends linearly on the spin four-vector of the outgoing nucleon  $S_N^\mu$ . The angles  $\theta_R$  and  $\phi_R$  define the direction of the bound nucleon spin  $\mathbf{s}_L$  in the frame in which the bound nucleon is at rest. In Appendix B we show explicit expressions for the antisymmetric parts of the single-nucleon tensors  $\mathcal{W}^{\mu\nu}$ ,  $\mathcal{Z}^{\mu\nu}$  and  $\mathcal{R}^{\mu\nu}$  for different current operators. Explicit expressions for their symmetric parts were already presented in [17].

In analogy to the standard PWIA, where the cross section factorizes into a single-nucleon cross section and the momentum distribution corresponding to a non-relativistic bound orbital, within RPWIA one may also introduce single-nucleon cross sections  $\sigma_{uu}^{eN}$ ,  $\sigma_{vv}^{eN}$  and  $\sigma_{uv}^{eN}$ , which are constructed by contracting the single-nucleon tensors  $\mathcal{W}^{\mu\nu}$ ,  $\mathcal{Z}^{\mu\nu}$  and  $\mathcal{N}^{\mu\nu}$  appearing in the three hadronic tensor contributions in Eqs. (4-6) with the leptonic tensor  $\eta_{\mu\nu}$  (see [17] for details). Then the differential cross section within RPWIA can be written as

$$\frac{d\sigma}{d\varepsilon' d\Omega_e d\Omega_N} = \frac{p_N M_N M_B}{M_A f_{rec}} \left[ \sigma_{uu}^{eN} N_{uu}(p) + \sigma_{vv}^{eN} N_{vv}(p) + \sigma_{uv}^{eN} N_{uv}(p) \right], \quad (12)$$

where  $\sigma_{uu}^{eN}$  is the free polarized electron-nucleon cross section already appearing in the standard PWIA analysis. Here  $\sigma_{vv}^{eN}$  and  $\sigma_{uv}^{eN}$  are new components that arise only because of the negative-energy projections and that may only appear in scattering from a bound nucleon. As already mentioned, this constitutes an important difference between PWIA and RPWIA. Whereas in PWIA the differential cross section factorizes into two terms, the electron-nucleon



cross section and the spectral function, in RPWIA the differential cross section depends on both positive- and negative-energy projections of the relativistic bound nucleon wave function. This result breaks the factorization property in the sense described in PWIA, namely, a clear separation into two terms, one describing the electron-nucleon scattering and the other connected to the nuclear structure of the target.

Within RPWIA one may also use the decomposition of currents into longitudinal and transverse components and then introduce the single-nucleon responses  $\mathcal{R}_{uu}^{k,k'}$ ,  $\mathcal{R}_{vv}^{k,k'}$  and  $\mathcal{R}_{uv}^{k,k'}$  that are given by taking the appropriate components of the single-nucleon tensors  $\mathcal{W}^{\mu\nu}$ ,  $\mathcal{Z}^{\mu\nu}$  and  $\mathcal{N}^{\mu\nu}$ , as is done in PWIA. The hadronic response functions can be written in RPWIA in the form

$$R^\alpha = R_P^\alpha + R_N^\alpha + R_C^\alpha, \quad (13)$$

where the three components are given by

$$R_P^\alpha = \mathcal{R}_{uu}^\alpha N_{uu}(p) \quad (14)$$

$$R_N^\alpha = \mathcal{R}_{vv}^\alpha N_{vv}(p) \quad (15)$$

$$R_C^\alpha = \mathcal{R}_{uv}^\alpha N_{uv}(p) \quad (16)$$

with  $\alpha = L, T, TL, TT, T', TL'$ . In standard PWIA only the responses  $\mathcal{R}_{uu}^\alpha$  occur.

To finish the discussion in this section, let us present some brief comments on the transferred polarization  $\mathbf{P}'$ . This is basically given as the ratio between the recoil nucleon polarized responses and the unpolarized responses. In particular, their three components  $P'_l$ ,  $P'_s$  and  $P'_n$  are given as

$$P'_{l,s} = \frac{(v_{T'} R_{l,s}^{T'} + v_{TL'} R_{l,s}^{TL'}) \cos \phi}{v_L R_0^L + v_T R_0^T + v_{TL} R_0^{TL} \cos \phi + v_{TT} R_0^{TT} \cos 2\phi} \quad (17)$$

$$P'_n = \frac{v_{TL'} R_n^{TL'} \sin \phi}{v_L R_0^L + v_T R_0^T + v_{TL} R_0^{TL} \cos \phi + v_{TT} R_0^{TT} \cos 2\phi}. \quad (18)$$

Note that  $P'_n$  only contributes for out-of-plane kinematics. The transferred polarization, as a ratio observable, is very well-suited in experimental studies to minimizing systematic errors. Different aspects of the underlying dynamics can be revealed when studying such observables than when considering the responses themselves; for instance, concepts such as the overall normalization of the cross section and responses connects to issues of spectroscopic factors, and such normalizations largely drop out when forming ratios of observables. Thus, such transferred polarizations hold promise for shedding light on other aspects of the problem such as the roles played by FSI and by both kinematical and dynamical relativistic effects. A full RDWIA analysis is surely needed before general remarks on the sensitivity of  $\mathbf{P}'$  to FSI could be presented and work along these lines is presently in progress [32].

### 3 Analysis of the results

In this section we present the results obtained as functions of the missing momentum  $p$ , for the various recoil nucleon polarization observables corresponding to proton knockout from

the  $p_{1/2}$  and  $p_{3/2}$  shells in  $^{16}\text{O}$  leading to the residual nucleus  $^{15}\text{N}$ . Four different kinematical situations have been selected:

1.  $q = 500 \text{ MeV}/c$ ,  $\omega = 131.56 \text{ MeV}$ ;
2.  $q = 1 \text{ GeV}/c$ ,  $\omega = 445 \text{ MeV}$ ;
3.  $\theta_N = 0$ ,  $p_N = 490 \text{ MeV}/c$ ;
4.  $\theta_N = 0$ ,  $p_N = 1 \text{ GeV}/c$ .

Kinematics 1 and 2 correspond to  $(q, \omega)$ -constant kinematics (sometimes also referred as quasi-perpendicular kinematics). In both cases the value selected of the transfer energy  $\omega$  corresponds almost to the quasielastic peak value (the scaling variable  $y$  is equal to zero in this situation), where one expects the validity of the impulse approximation in describing the electron scattering process to be the highest. The interest in selecting these two kinematics is twofold. First, the dynamical relativistic effects for the unpolarized responses have been already analysed in [17] for kinematics 1. Secondly, kinematics 2 roughly corresponds to that used in the experiments E89-003 [33] and E89-033 [34] performed at JLab. Kinematics 3 and 4 correspond to parallel kinematics where the recoil nucleon momentum  $\mathbf{p}_N$  is detected parallel to the transfer momentum  $\mathbf{q}$ . The kinetic energy of the outgoing nucleon is also fixed, as well as the electron beam energy. Within parallel kinematics let us recall that positive values of the missing momentum  $p$  correspond to  $\theta = 0$ , i.e.,  $\mathbf{p}$  and  $\mathbf{q}$  are parallel, whereas negative  $p$ -values correspond to  $\theta = \pi$ , i.e.,  $\mathbf{p}$  and  $\mathbf{q}$  antiparallel.

It is important to remark that each of the types of kinematics,  $(q, \omega)$ -constant and parallel, presents clear differences that may lead to significant effects in the polarization observables. Within  $(q, \omega)$ -constant kinematics, varying the missing momentum  $p$  means changing the direction in which the outgoing nucleon is detected. The kinetic energy of the outgoing nucleon should also vary to fulfill energy conservation, although this variation is negligible in most of the cases (see discussion in [35]). Within parallel kinematics, varying the missing momentum  $p$  means changing the value of the transfer momentum  $q$ . Although the transfer energy  $\omega$  also depends on  $p$ , its variation in the range,  $-200 \leq p \leq 300 \text{ MeV}/c$ , is almost negligible since  $M_B \gg p$ , meaning that as  $p$  varies one is moving far away from the quasielastic peak (QEP). This is in contrast with the previous kinematics where one is always at the center of the QEP. A very general and systematic study of the different ingredients that enter in the analysis of the kinematics of coincidence electron scattering reactions has been presented in [28].

As has been discussed at length in previous work [17, 31, 36], the choice of the nucleon current operator  $J^\mu$  that enters in the description of  $(e, e'N)$  processes is to some extent arbitrary. In this work we have considered the two choices of the current operator known as  $CC1$  and  $CC2$ . Moreover, the current is not conserved and different gauges should be considered: i) Landau ( $NCC1$ ,  $NCC2$ ) - no current conservation imposed, ii) Coulomb ( $CC1^{(0)}$ ,  $CC2^{(0)}$ ) - current conservation imposed by eliminating the third component, and iii) Weyl ( $CC1^{(3)}$ ,  $CC2^{(3)}$ ) - current conservation imposed by eliminating the time component. This subject is studied in detail in Section 3.1 where we show the behaviour of the polarized single-nucleon responses insofar as their dependence on the current-conservation prescription

selected is concerned. We present results for the positive-energy, as well as for the negative-energy components.

In Sections 3.2 and 3.3 we present the results for the polarized hadronic responses and transferred polarization asymmetries, respectively. The momentum distribution components in Eqs. (40-42) were studied in detail in [17, 37] for the  $p_{1/2}$  and  $p_{3/2}$  shells in  $^{16}\text{O}$ . As shown there, the positive-energy projections are clearly dominant at low  $p$ , while for  $p > 300$  MeV/c the negative-energy projections start to play an important role and the differences between off-shell prescriptions are enhanced. Moreover, the behaviour of the dynamical enhancement function  $\beta_\kappa$  in Eq. (44) for stretched ( $p_{3/2}$ ) and jack-knifed ( $p_{1/2}$ ) states is quite different. This explains why the amplitudes of the negative-energy projections for the  $p_{1/2}$  state are much larger than those for the  $p_{3/2}$ . All of the results presented in Sections 3.2 and 3.3 correspond to a bound state wave function computed within the Walecka relativistic model [38] using the parameters of the set HS [39, 40]. Results with the NLSH [41] and NL3 [42] sets are quite similar and a discussion of those would follow the same trends.

### 3.1 Polarized single-nucleon responses

In Figs. 1 and 2 we show the behaviour of the recoil nucleon polarized single-nucleon responses. For brevity in this work we consider only coplanar kinematics, i.e.,  $\phi = 0$ , which means that only four recoil nucleon polarized responses are accessible,  $R_{l,s}^{T'}$  and  $R_{l,s}^{TL'}$ . For each single-nucleon response we show the results for the positive-energy  $uu$  (left-hand panels), and negative-energy  $uv$  (middle panels) and  $vv$  (right-hand panels) contributions. Curves for the six off-shell prescriptions are shown in all of the cases.

#### Analysis in $(q, \omega)$ -constant kinematics

We start our discussion with the case of  $(q, \omega)$ -constant kinematics. For simplicity we only show results corresponding to kinematics 1 (Fig. 1). The analysis of kinematics 2 follows in general similar trends. Let us consider first the two purely transverse polarized responses  $\mathcal{R}_{l,s}^{T'}$ . These responses only depend on the current operator ( $CC1$  vs  $CC2$ ) selected, i.e., they are not affected by gauge ambiguities. Fig. 1 shows that, while the positive-energy components  $(\mathcal{R}_{l,s}^{T'})_{uu}$  obtained with the two currents are rather similar, the negative-energy contributions  $(\mathcal{R}_{l,s}^{T'})_{uv}$  and  $(\mathcal{R}_{l,s}^{T'})_{vv}$  deviate significantly, especially for the latter. This behaviour was already observed for the purely transverse unpolarized single-nucleon responses  $\mathcal{R}^T$  and  $\mathcal{R}^{TT}$  (see discussion in [17]). Although not shown, the same qualitative behaviour is found for kinematics 2.

Comparing the results obtained for the negative-energy components with the positive-energy ones, we observe that the  $uv$  and  $vv$  contributions are clearly maximized by the  $CC1$  current operator. This is also consistent with the results obtained for the unpolarized responses and reflects a stronger dependence in general on the negative-energy projections  $\beta_\kappa$  when using the  $CC1$  operator. It is also interesting to observe the different contributions of the  $uv$  and  $vv$  components in both transverse responses  $\mathcal{R}_l^{T'}$  and  $\mathcal{R}_s^{T'}$ . The negative-energy ( $uv$  and  $vv$ ) contributions compared with the positive-energy ( $uu$ ) one are considerably larger for  $\mathcal{R}_s^{T'}$ . This result will be discussed further in next section, when we show the total

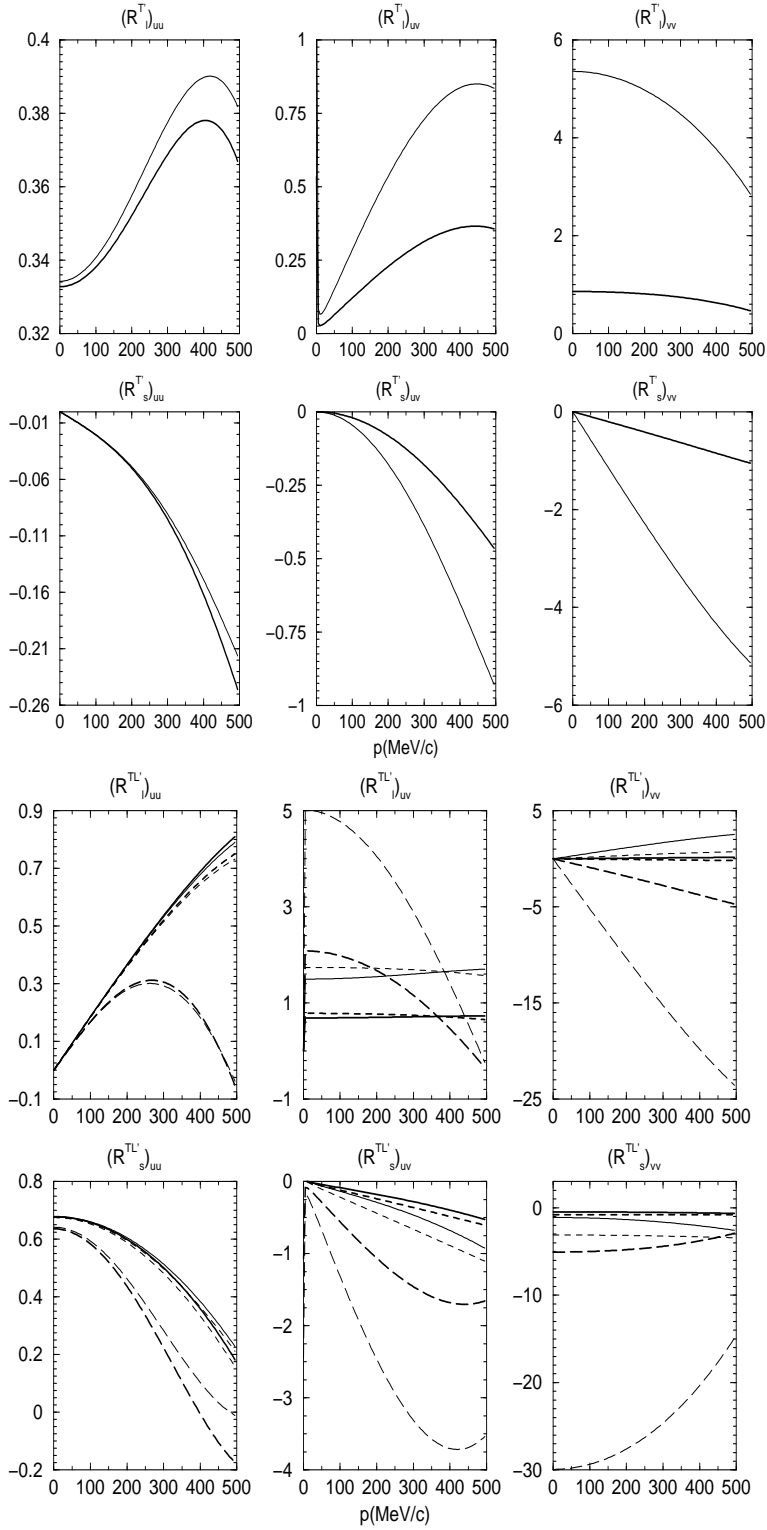


Figure 1: Polarized single-nucleon response functions for kinematics 1 (see text). The two top panels correspond to the purely transverse  $T'$  responses, while the two bottom ones show results for  $TL'$  responses. Thick lines correspond to prescriptions based on the  $CC2$  current operator and thin lines to the  $CC1$  current. Results are shown for Landau ( $NCC1/NCC2$ ) (solid lines), Coulomb ( $CC1^{(0)}/CC2^{(0)}$ ) (short-dashed lines) and Weyl ( $CC1^{(3)}/CC2^{(3)}$ ) (long-dashed lines) gauges.

Response	$\alpha_2^P$	$\alpha_2^C$
$L$	$1.4(n = 0)$	$0.1(n = 1)$
$T$	$1.2(n = 0)$	$0.1(n = 1)$
$TL$	$0.3(n = 1)$	$1.2(n = 0)$
$TT$	$0.1(n = 2)$	$0.7(n = 1)$
$T'_l$	$1.1(n = 0)$	$-0.3(n = 1)$
$TL'_l$	$-0.1(n = 1)$	$0.2(n = 0)$
$T'_s$	$3.3(n = 1)$	$0.004(n = 2)$
$TL'_s$	$-1.4(n = 0)$	$0.2(n = 1)$

Table 1: Coefficients  $\alpha_2$  given by the decomposition in Eq. (19) for the positive and crossed response functions.

hadronic responses.

The interference  $TL'$  polarized responses are shown in the two bottom panels of Fig. 1. In this case, the responses depend on the gauge and hence six different curves corresponding to the six ‘off-shell’ prescriptions considered are presented. From these, the  $CC1^{(3)}$  and  $CC2^{(3)}$  choices cause large deviations in all of the components, including the positive-energy ones. On the contrary, the four remaining prescriptions give very similar results for the  $uu$  component, deviating clearly in the case of the negative-energy components, particularly when comparing results corresponding to prescriptions using the two current operators  $CC1$  and  $CC2$ . In analogy with the two  $T'$  responses, the  $CC1$  choice maximizes the ‘off-shell’ ambiguities, as well as the contribution of the  $uv$  and  $vv$  components compared with the positive-energy one. Finally, note that the relative contribution of the negative-energy components is more important for the  $\mathcal{R}_l^{TL'}$  response. As will be shown in next section, this means that the hadronic response  $R_l^{TL'}$  can be more sensitive to dynamical relativistic effects than  $R_s^{TL'}$ .

In [28] we introduced the concept of class number and its connection with the analysis of the kinematical relativistic effects. Here we extend that to include also the  $uv$ -cross contributions ( $C$ ), i.e., dynamical relativistic effects. To make clearer the discussion that follows, let us rewrite the response functions according to the generic form at low- $\chi$ :

$$\mathcal{R} = \chi^n \alpha_0 [1 + \alpha_2 \chi^2 + \mathcal{O}(\chi^4)], \quad (19)$$

where  $\chi \equiv (p/M_N) \sin \theta$  and  $n = 0, 1, 2$  labels the class type “0”, “1”, “2”, etc (see [28] for details).

Truncating all expansions of the above type at terms involving  $\alpha_2$  the results obtained are presented in table 1. We compare the cross ( $C$ ) contributions with the PWIA results (labelled “ $P$ ”). In [28] we have shown that kinematical relativistic effects are typically larger for class “0” responses than for responses of classes “1” and “2”. Now an extended pattern emerges for the terms of type “ $C$ ” involving dynamical relativistic effects. First, two groups occur, one in which the class of the  $C$  contribution is one higher than the class of the  $P$  contribution ( $L, T, T'_l, T'_s$  and  $TL'_s$ ), and another in which the class of the  $C$  contribution is one lower than the class of the  $P$  contribution ( $TL, TT$  and  $TL'_l$ ). In the latter cases

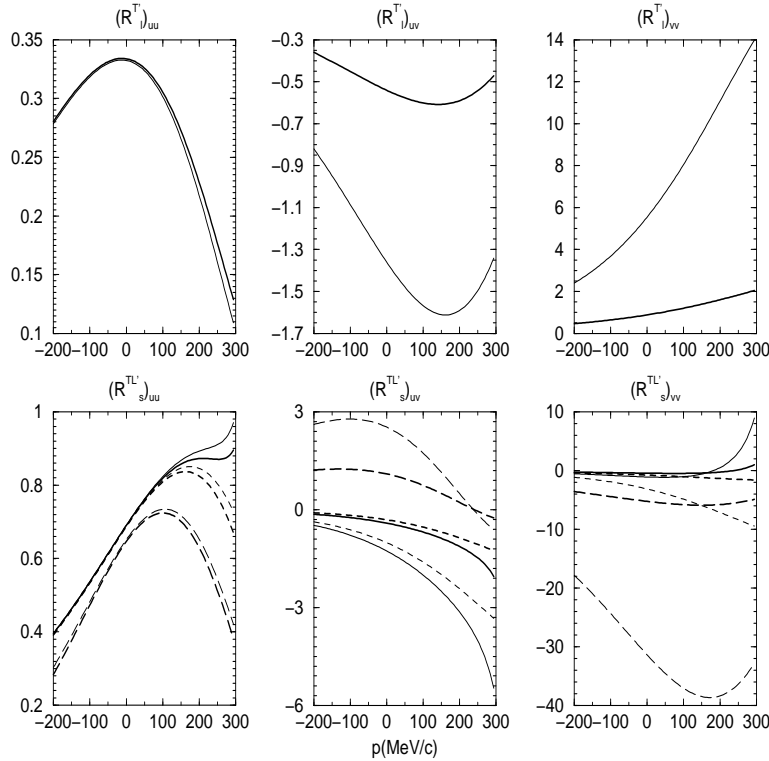


Figure 2: Polarized single-nucleon responses in parallel kinematics 3. The labeling of the curves is as in Fig. 1.

we expect to see greater consequences of dynamical relativity than in the former. Second, we see from above that the importance of higher-order terms in the  $\chi^2$  expansions for type  $C$  typically correlates in the same way it does for the  $P$  expansions: the class “0” cases generally show larger effects than do the responses in classes “1” and “2”.

### Analysis in parallel kinematics

Fig. 2 shows the results for parallel kinematics where only two polarized responses survive, namely  $\mathcal{R}_l^{T'}$  and  $\mathcal{R}_s^{TL'}$ . In this case the positive- and negative-energy components of the polarized response  $\mathcal{R}_l^{T'}$  are proven to be identical to the respective components of the unpolarized transverse response  $\mathcal{R}_0^T$ . In fact, these two responses are identical in parallel kinematics for  $j = 1/2$  orbits even including FSI in the analysis (see [19, 29] for details). Here we only present the results corresponding to kinematics 3. The discussion and analysis of responses for kinematics 4 follow in general similar trends. Some of the points discussed for the previous kinematics can be also applied here. In particular, note that the two current operators give very similar results for the positive-energy component of  $\mathcal{R}_l^{T'}$ , whereas they differ strongly for the negative-energy contributions, being maximized for the  $CC1$  current operator. In the case of  $\mathcal{R}_s^{TL'}$ , the  $CC1^{(3)}$  and  $CC2^{(3)}$  prescriptions produce the biggest differences even for the  $uu$  component. Again, choices based on the  $CC1$  current maximize the role of the negative-energy contributions.

It is interesting to remark that the two single-nucleon responses surviving in parallel kinematics are the ones that also show less sensitivity to dynamical relativistic effects in  $(q, \omega)$ -constant kinematics (Fig. 1). However, by looking more carefully at the relative contributions to these two responses of the negative-energy  $uv$  and  $vv$  components, the sensitivity is shown to be more significant in the case of parallel kinematics. We will return to this issue in the next section when showing the behaviour of the total hadronic responses.

To finish the discussion on parallel kinematics we should also point out the basic differences observed in the results for positive and negative  $p$ -values. As explained above, positive (negative)  $p$ -values mean parallel (antiparallel) direction between  $\mathbf{p}$  and  $\mathbf{q}$ . From the responses shown in Fig. 2, one observes that ‘off-shell’ ambiguities are considerably reduced for  $p$ -negative. This fact is maintained for the positive-energy, as well as for the negative-energy components. One can also observe that the relative contribution of  $uv$  and  $vv$  components, compared with  $uu$ , although important is also reduced in the case of negative  $p$ -values. From these results, it is clear that the negative- $p$  region should be favoured in the experiments. This coincides with the conclusions presented in [25]. In general, response functions seem to be less affected by ‘off-shell’ uncertainties in that case (see [28]), although relativistic dynamical effects are still important.

## 3.2 Hadronic responses

In this section we present results for the recoil nucleon polarized hadronic responses as defined in Eq. (13). Our aim is to analyze the relative importance of the negative-energy projection contributions for the various ‘off-shell’ prescriptions considered. As already mentioned, we consider the cases of the proton being knocked out from the  $p_{1/2}$  and  $p_{3/2}$  shells in  $^{16}\text{O}$ .

### Analysis in $(q, \omega)$ -constant kinematics

In Fig. 3 we show the total hadronic responses for  $p_{1/2}$  and  $(q, \omega)$ -constant kinematics. The top panels correspond to kinematics 1 and the bottom panels to kinematics 2. As we see, apart from quantitative details, the behaviour of the responses is quite similar for the two choices of kinematics, and accordingly the discussion that follows applies to both. Concerning the purely transverse  $T'$  responses, we observe that the ambiguity introduced by the choice of current operator at the maxima of the responses ( $p \sim 100$  MeV/c, as our results are obtained for p-waves), although visible in the two responses, is larger in the case where the spin polarization lies in the sideways direction (for the  $R_s^{T'}$  response it is  $\sim 16\%$  for kinematics 1 and  $\sim 4\%$  for kinematics 2, while for  $R_l^{T'}$  is  $\sim 7\%$  for kinematics 1 and  $\sim 2\%$  for kinematics 2). Note however, that in absolute value  $R_s^{T'}$  is more than one order of magnitude smaller than  $R_l^{T'}$ . The reason for the ‘off-shell’ uncertainty in these responses can be traced back to the influence of the negative-energy projections of the bound nucleon wave function, given by the contribution of the crossed and negative components introduced in Eq. (13). In fact, although not shown in the graphs, we have checked that for the positive terms there is almost no difference between the results provided by the two current operators selected, whereas the crossed and negative terms strongly depend on the current choice, explaining the differences observed in Fig. 3. The relative influence introduced by these terms at the

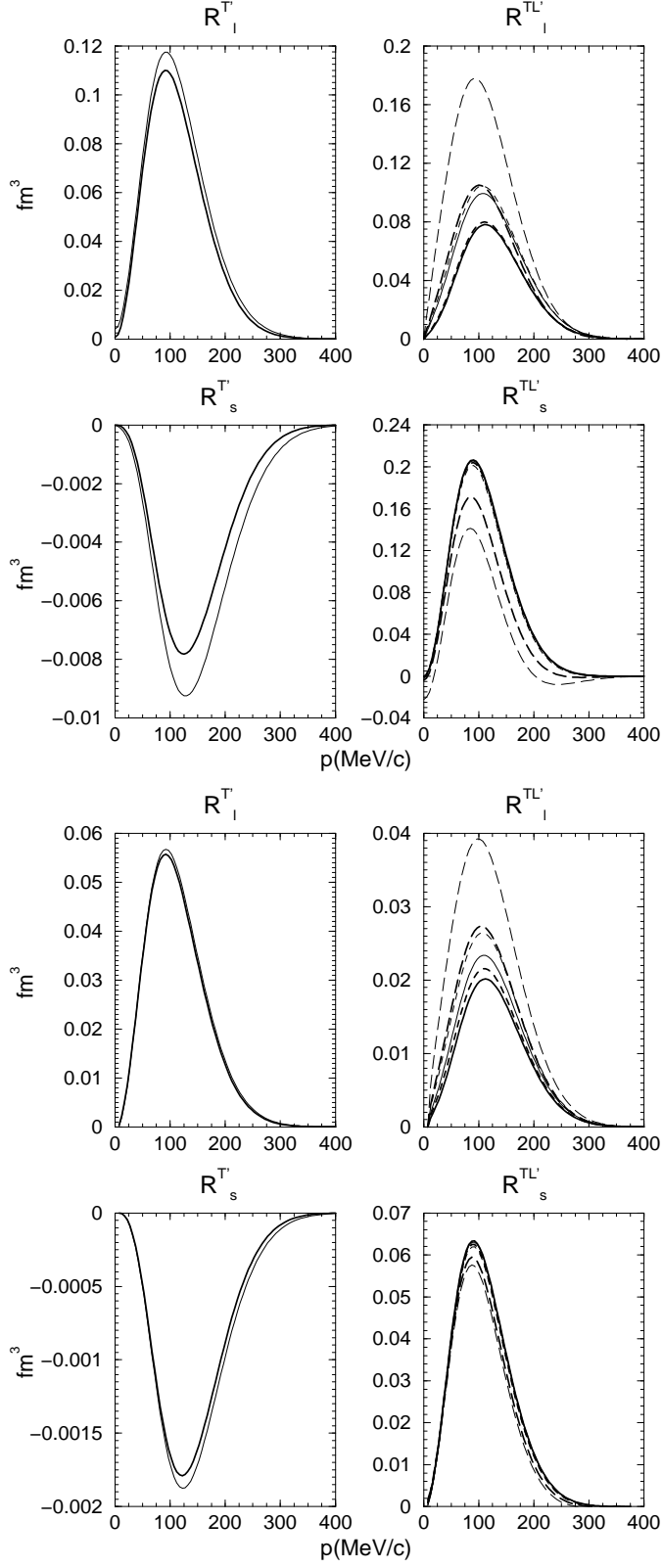


Figure 3: Polarized hadronic response functions for the  $p_{1/2}$  shell in  $(q, \omega)$ -constant kinematics. Top panels correspond to kinematics 1 and bottom panels to kinematics 2 (see text). The curves are labelled as in Fig. 1.



maxima is  $\sim 10\%$  ( $\sim 4\%$ ) for  $CC1$  ( $CC2$ ) choices in  $R_i^{T'}$ , and  $\sim 30\%$  ( $\sim 11\%$ ) for  $CC1$  ( $CC2$ ) in  $R_s^{T'}$  in the case of kinematics 1, and  $\sim 3\%$  ( $\sim 1\%$ ) for  $CC1$  ( $CC2$ ) in  $R_i^{T'}$ , and  $\sim 9\%$  ( $\sim 4\%$ ) for  $CC1$  ( $CC2$ ) in  $R_s^{T'}$  in the case of kinematics 2. These numbers explain not only why the ‘off-shell’ ambiguity at the maxima of the responses is larger for  $R_s^{T'}$  than for  $R_i^{T'}$ , but also why it is significantly reduced in the case of kinematics 2. We have also considered higher values of  $q$  to verify that as  $q$  increases off-shell effects diminish.

The polarized interference transverse-longitudinal responses  $R_i^{TL'}$  and  $R_s^{TL'}$  are shown for the six ‘off-shell’ prescriptions in the right-hand panels of Fig. 3. It is interesting to note the different behaviour shown by the various prescriptions in the two responses. For  $R_s^{TL'}$  only the Weyl gauge prescriptions and particularly the  $CC1^{(3)}$  case produce significant differences (larger for kinematics 1) with respect to the other prescriptions. Results corresponding to Landau and Coulomb gauges with  $CC1$  and  $CC2$  currents are very similar. As before, these facts are directly associated with the role that the negative-energy projection components play in each case. For Landau and Coulomb gauge prescriptions the role played by the NEP in this response is less than  $\sim 4\%$ . In contrast, the negative-energy contribution for the Weyl prescriptions are  $\sim 28\%$  for  $CC1^{(3)}$  and  $\sim 10\%$  for  $CC2^{(3)}$  for kinematics 1, and  $\sim 8\%$  for  $CC1^{(3)}$  and  $\sim 3\%$  for  $CC2^{(3)}$  for kinematics 2. However, it must be pointed out that this choice of gauge leads to significantly different results even in the positive components.

The case of the  $R_i^{TL'}$  response is clearly different. Here the spread amongst the six ‘off-shell’ prescriptions is wider. Not only does the Weyl gauge give rise to different results, but also the responses corresponding to the two Landau gauge prescriptions ( $NCC1$ ,  $NCC2$ ) differ from the ones corresponding to Coulomb ( $CC1^{(0)}$ ,  $CC2^{(0)}$ ). Interestingly, once one has selected the current operator, the results obtained with both Coulomb and Landau gauges are very similar in the case of kinematics 1, while the differences between them increase for kinematics 2, particularly for  $CC1$  current. Moreover, the effects introduced by the current choice for the Coulomb and Landau gauges, although visible, are much smaller than in the case of the Weyl gauge where the difference between  $CC1^{(3)}$  and  $CC2^{(3)}$  amounts to a factor  $\sim 1.7$  (kinematics 1) and  $\sim 1.4$  (kinematics 2). All of these effects in  $R_i^{TL'}$  can be traced back to the behaviour of its various positive- and negative-energy components. The contributions given by the six prescriptions in the crossed components are similar or even considerably larger ( $CC1^{(3)}$ ) than the ones corresponding to the positive-energy terms — from  $\sim 35\%$  ( $NCC2$ ,  $CC2^{(0)}$ ) up to  $\sim 250\%$  ( $CC1^{(3)}$ ) for kinematics 1, and from  $\sim 35\%$  ( $NCC2$ ) up to  $\sim 180\%$  ( $CC1^{(3)}$ ) for kinematics 2. Moreover, the spread of the ‘off-shell’ ambiguities in the negative-energy terms is much wider than in the positive-energy contribution. These facts explain on one hand why the total  $R_i^{TL'}$  response is much bigger than its purely positive-energy contribution and on the other why the off-shell uncertainties are so large.

Summarizing, we conclude that the polarized response  $R_i^{TL'}$  seems to present the highest sensitivity to the relativistic dynamical enhancement of the lower components of the bound nucleon wave function. Unfortunately, the ‘off-shell’ uncertainty is consequently the largest. The transverse response  $R_s^{T'}$  also shows significant sensitivity to dynamical relativistic effects; however it is very small and hence difficult to measure. Finally,  $R_s^{TL'}$  and  $R_i^{T'}$  show less sensitivity to the negative-energy contributions, and present the lowest spread due to ‘off-shell’ uncertainties. At the maxima of the responses, the off-shell ambiguity in the two purely transverse responses  $R_{i,s}^{T'}$  is significantly reduced for increasing  $(q, \omega)$ -values (within

the QEP). Concerning the interference  $R_{i,s}^{TL'}$  responses, the off-shell effects corresponding to the Landau and Coulomb gauges remain quite similar when varying  $q$  (under quasielastic conditions).

The role played by the negative-energy projection components in the four polarized responses is more clearly seen in Fig. 4, where we present the results corresponding to the Coulomb gauge using the  $CC1$  and  $CC2$  choices of the current and kinematics 1. Results for the Landau gauge are seen to be very similar. We show the fully-relativistic result (solid) versus its three contributions as given by Eqs. (14-16):  $R_P^\alpha$  (dotted),  $R_C^\alpha$  (short-dashed) and  $R_N^\alpha$  (long-dashed). Note that  $R_C^\alpha$  and  $R_N^\alpha$  both come from the negative-energy projection contributions. The dynamical relativistic effects are easily appreciated by just comparing the  $N$  and  $C$  terms with the total response. In the case of the  $CC1^{(0)}$  prescription (two top panels), it is clearly observed that in two responses,  $R_i^{T'}$  and  $R_s^{TL'}$ , the contribution of the negative-energy projections is almost negligible, that is, dynamical relativistic effects from the bound nucleon wave function do not significantly affect these responses. On the contrary, the two remaining polarized responses,  $R_s^{T'}$  and  $R_i^{TL'}$ , are much more sensitive. In both cases, although the  $N$  term does not contribute significantly to the total result, the crossed term  $C$  plays an important role, particularly for the  $R_i^{TL'}$  response where, as already discussed, its contribution is similar to the one coming from the positive-energy projection. This result resembles what appeared for the unpolarized interference  $TL$  response [17]. Hence there exists a strong discrepancy between RPWIA results and those corresponding to the standard PWIA (we must recall that although the positive-energy term in Eq. (14) is not identical to the PWIA result, for which we must take the non-relativistic momentum distribution  $N_{nr}(p)$ , the difference is very small provided that  $N_{nr}(p) \sim N_{uu}(p)$ ). As shown in the two bottom panels of Fig. 4, the results obtained for the Coulomb gauge with the  $CC2$  nucleon current operator follow a similar trend to the ones discussed for the  $CC1$  case, except for the magnitude of the relativistic effects. Although the role of the  $N$  and crossed  $C$  terms is significantly reduced for the  $CC2$  current, their effects are still quite sizeable in  $R_s^{T'}$  and  $R_i^{TL'}$ . This general behaviour is similar to the one already stated for the unpolarized responses in [17]. Finally, although not shown here for simplicity, we have also explored the results obtained for kinematics 2. We prove that dynamical relativistic effects in  $\mathcal{R}_i^{TL'}$  are shown to be independent of  $q$ , under QE conditions, when the  $CC1^{(0)}$  prescription is used. In the case of  $CC2^{(0)}$  the role of the negative-energy components increases slightly as  $q$  goes to higher values. On the contrary, for the two purely transverse responses  $R_{i,s}^{T'}$ , dynamical relativistic effects are significantly reduced as  $(q, \omega)$ -values increase.

In what follows we analyze the case of the  $p_{3/2}$  shell and  $(q, \omega)$ -constant kinematics. For simplicity we only consider kinematics 1, the behaviour of the responses for kinematics 2 being similar. We have checked (not shown here) that the four hadronic responses obtained for the various off-shell prescriptions, compared with the case of the  $p_{1/2}$  orbit (Fig. 3), present a much smaller ‘off-shell’ uncertainty. This is connected with the minor role played by the negative-energy projection components. Despite the fact that the ‘off-shell’ uncertainties for  $R_C^\alpha$  and  $R_N^\alpha$  in Eq. (13) are of the same order of magnitude as in the case of the  $p_{1/2}$  shell, their relative contribution in the total hadronic responses is much reduced; only for the  $R_i^{TL'}$  response is the contribution of the negative-energy projections significant. This arises from the interestingly different behaviour of the lower components in the two cases, namely, that

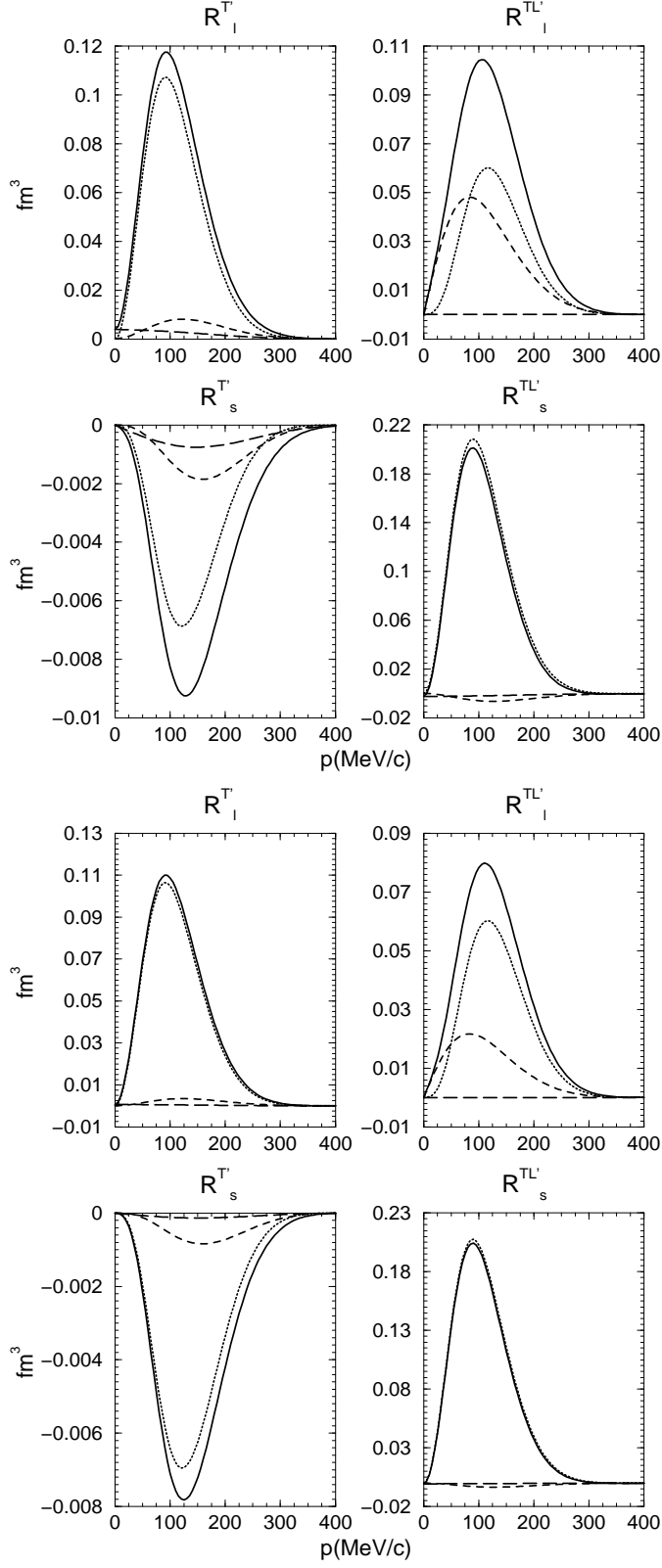


Figure 4: Hadronic response functions for the  $1p_{1/2}$  shell and kinematics 1. Top panels correspond to the  $CC1^{(0)}$  prescription and bottom panels to  $CC2^{(0)}$ . The fully-relativistic response (solid line) is compared with the three components:  $R_P^\alpha$  (dotted line),  $R_C^\alpha$  (short-dashed line) and  $R_N^\alpha$  (long-dashed line).

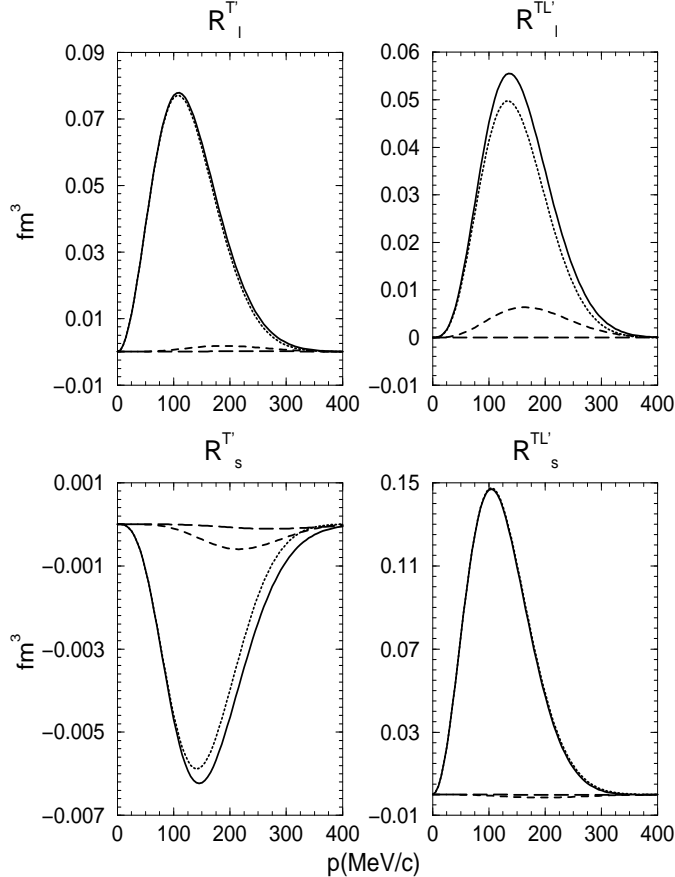


Figure 5: Hadronic response functions for the  $1p_{3/2}$  shell and kinematics 1 using the  $CC1^{(0)}$  prescription. The fully-relativistic response (solid line) is compared with the three components:  $R_P^\alpha$  (dotted line),  $R_C^\alpha$  (short-dashed line) and  $R_N^\alpha$  (long-dashed line).

the  $p_{1/2}$  case (“jack-knifed”) has lower components that have an  $s_{1/2}$  nature, whereas the  $p_{3/2}$  case (“stretched”) has lower components that go as  $d_{3/2}$ .

The role of the negative-energy components is more clearly seen in Fig. 5 where the terms  $R_P^\alpha$ ,  $R_C^\alpha$  and  $R_N^\alpha$  are plotted separately and compared with the fully-relativistic results. The  $CC1$  current, which magnifies dynamical relativistic effects, and the Coulomb gauge have been chosen. Note that the positive contributions are very similar to the full responses. This result agrees with the general study presented in [37] where the role of the lower components of the bound nucleon wave function was investigated for different spin-orbit partner shells. In [37] it was proven that the large deviation produced by different ‘off-shell’ prescriptions in the unpolarized responses  $R^{TL}$  and  $R^{TT}$  takes place for the jack-knifed states, but not for the stretched states. This result, which also persists for the recoil nucleon polarized responses, can be understood by the different behaviour of the dynamical enhancement function  $\beta_\kappa$  in Eq. (44) for the stretched and jack-knifed states.

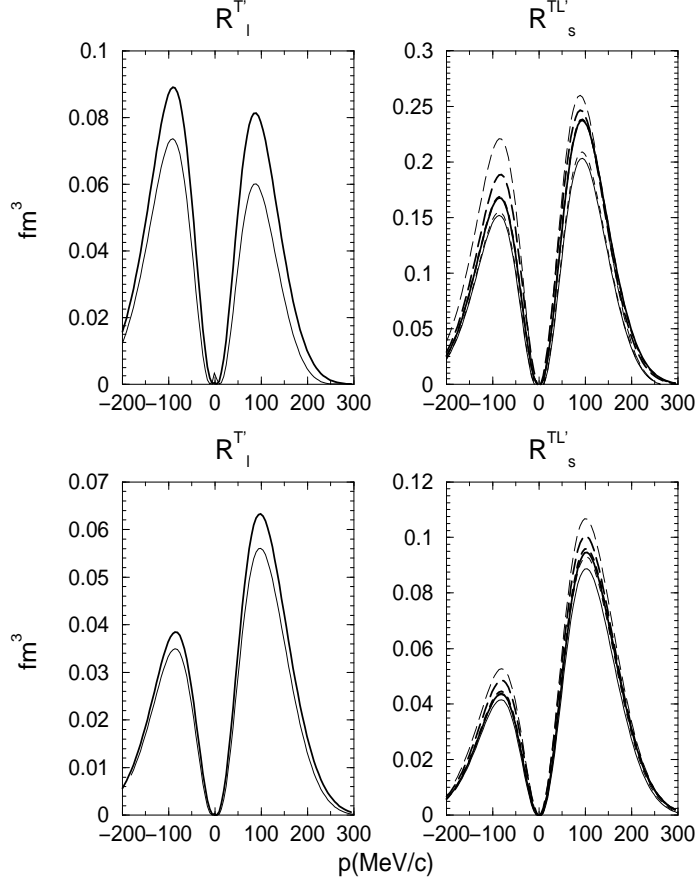


Figure 6: Polarized hadronic response functions for the  $1p_{1/2}$  shell in parallel kinematics. Top panels correspond to kinematics 3 and bottom panels to kinematics 4 (see text). The curves are labelled as in Fig. 1.

### Analysis in parallel kinematics

To finish the discussion in this section, we consider the case of parallel kinematics. We only show results for proton knock-out from the  $p_{1/2}$  shell, as the discussion of the  $p_{3/2}$  orbit case follows similar trends to the ones already presented for  $(q, \omega)$ -constant kinematics. The two surviving responses,  $R_l^{T'}$  and  $R_s^{TL'}$ , are shown in Fig. 6 for the various ‘off-shell’ prescriptions. The top panels correspond to kinematics 3 and the bottom panels to kinematics 4. It is interesting to note that in the case of kinematics 4, i.e., higher outgoing nucleon kinetic energy, the asymmetry in the responses for positive and negative  $p$ -values is significantly enhanced, although this result is already present at the level of the positive-energy contributions alone. Concerning the purely transverse  $T'$  response, we have seen that the significant ‘off-shell’ discrepancy observed at the maxima comes essentially from the crossed term, provided that both current operators  $CC1$  and  $CC2$  give the same positive-energy response. In contrast, the negative-energy contributions differ significantly, the  $CC1$  result being much bigger in absolute value. Moreover, the ambiguity (evaluated at the maxima of the responses,  $p \sim 100$  MeV/c) introduced by the current choice is larger in the region of positive  $p$ -values,  $\sim 27\%$  ( $\sim 11\%$ ) for kinematics 3 (kinematics 4), than for negative  $p$ ,

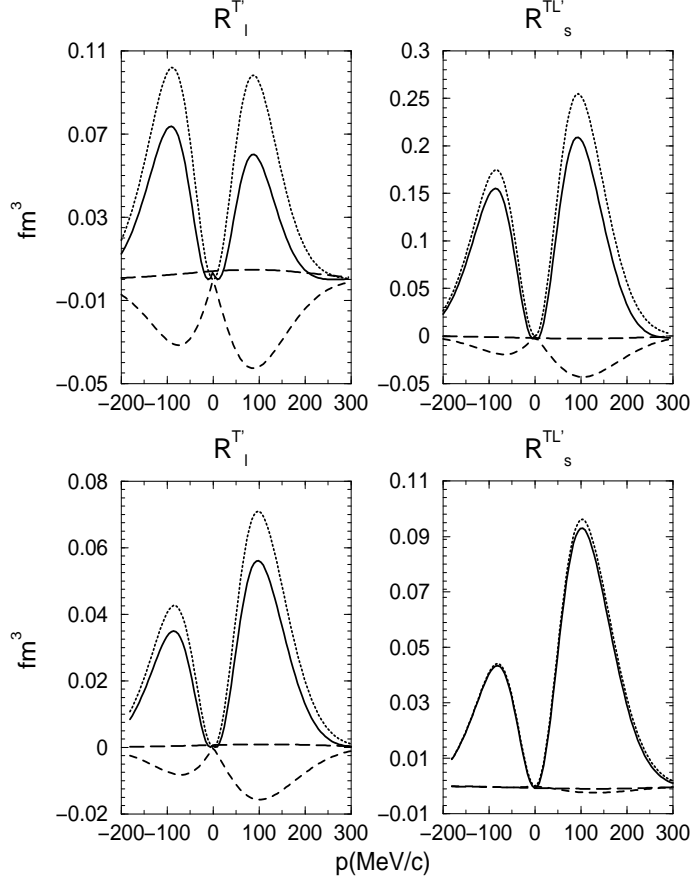


Figure 7: Hadronic response functions for the  $1p_{1/2}$  shell using the  $CC1^{(0)}$  prescription. The top panels correspond to kinematics 3 and the bottom ones to kinematics 4. The fully-relativistic response (solid line) is compared with the three components:  $R_p^\alpha$  (dotted line),  $R_C^\alpha$  (short-dashed line) and  $R_N^\alpha$  (long-dashed line).

$\sim 17\%$  ( $\sim 9\%$ ) for kinematics 3 (kinematics 4). Note that off-shell uncertainties are also reduced when the outgoing nucleon momentum is larger (kinematics 4). A similar behaviour is also observed for the  $R_s^{TL'}$  response in the case of the prescriptions based on Coulomb and Landau gauges. The positive-energy contribution is almost identical for these four ‘off-shell’ prescriptions, whereas significant differences appear in the negative-energy components, with the contributions based on the  $CC1$  current choice being much more important. Moreover, this off-shell spread is larger within the positive- $p$  region than for  $p$  negative. In the case of the Weyl gauge,  $CC1^{(3)}$  and  $CC2^{(3)}$ , the responses obtained differ from the ones corresponding to the Coulomb and Landau gauges, even at the level of the positive-energy projection component. Also the behaviour of the crossed term for the Weyl prescriptions is opposite (positive contribution) to the results of the other ‘off-shell’ prescriptions. Moreover, whereas the Coulomb and Landau results in the crossed component are larger (in absolute value) for  $p$ -positive, the results for the Weyl gauge are the opposite, i.e., larger contributions for  $p$ -negative. These results are directly connected with the behaviour of the single-nucleon responses shown in Fig. 2.

As in the previous choices of kinematics, in order to clarify the role of the negative-

energy projection components, we show in Fig. 7 the separate contribution of the terms  $R_P^\alpha$ ,  $R_C^\alpha$  and  $R_N^\alpha$  for the Coulomb gauge and  $CC1$  current choice. Results for Landau gauge and the same current are similar, while choosing the  $CC2$  current minimizes the negative-energy contributions. Comparing with the cases of  $(q, \omega)$ -constant kinematics (Fig. 4), we observe that the two surviving responses in parallel kinematics present (at their peaks) a stronger sensitivity to dynamical relativistic effects. From these results it seems to be clear that choosing parallel kinematics enhances the sensitivity to dynamical relativistic effects in the two surviving polarized responses compared with these same responses evaluated in  $(q, \omega)$ -fixed kinematics. The reason for this can be traced back to the general discussion on kinematics presented at the beginning of Section 3. Whereas for  $(q, \omega)$ -constant kinematics the  $\omega$ -value is chosen to fulfill the QEP condition, in parallel kinematics, varying  $p$  forces the transfer momentum  $q$  also to vary,  $\omega$  being practically constant. This means that one is moving away from the center of the QEP. As shown in [17] for the unpolarized responses, ‘off-shell’ uncertainties and dynamical relativistic effects increase as one moves far away from the QEP. This fact could also explain why the sensitivity of the responses to the negative-energy projections, evaluated at the maxima, is higher for kinematics 3:  $\sim 65\%$  vs  $\sim 27\%$  in  $R_l^{T'}$  and  $\sim 23\%$  vs  $\sim 3\%$  in  $R_s^{TL'}$  for  $p = 100$  MeV/c;  $\sim 37\%$  vs  $\sim 21\%$  in  $R_l^{T'}$  and  $\sim 12\%$  vs  $\sim 1\%$  in  $R_s^{TL'}$  for  $p = -100$  MeV/c. These results show that the dynamical enhancement of the lower components of the bound wave function have a greater effect in the case of positive  $p$ -values. Note that the maxima in the responses, located approximately at  $p = \pm 100$  MeV/c, correspond to values of the transfer momentum:  $q \approx 400$  MeV/c ( $q \approx 600$  MeV/c) for  $p$ -positive (-negative) and kinematics 3, and  $q \approx 900$  MeV/c ( $q \approx 1100$  MeV/c) for  $p$ -positive (-negative) and kinematics 4. In fact, we state without elaborating further that the relative sizes of the effects seen here appear to correlate with the value of  $|y|/q$ .

### 3.3 Transferred Polarization Asymmetries

In this section our aim is to analyze the behaviour of the transferred polarization asymmetries  $P_l'$  and  $P_s'$  introduced in Eq. (17). We discuss the uncertainty introduced by the various off-shell prescriptions and the role played by the dynamical enhancement of the lower components of the bound nucleon wave function. Let us recall that these transferred polarization observables are thought to be very special in that they have the potential to provide information on the nucleon form factors in the nuclear medium; hence a careful analysis of the ‘off-shell’ and relativistic effects is crucial before one can hope to gain such insight.

In Figs. 8 and 9 we show the results for  $P_l'$  and  $P_s'$  corresponding to kinematics 1 and 2, respectively. In both cases,  $p_{1/2}$  (left-hand panels) and  $p_{3/2}$  (right-hand panels) shells have been considered. Each graph presents six curves corresponding to the six ‘off-shell’ prescriptions discussed. Finally, in the case of kinematics 1 (Fig. 8), results are shown for forward and backward electron scattering angles:  $\theta_e = 30^\circ$  ( $\varepsilon = 1$  GeV) (bottom panels) and  $\theta_e = 150^\circ$  ( $\varepsilon = 324$  MeV) (top panels). For kinematics 2 (Fig. 9), only forward electron scattering ( $\theta_e = 23.4^\circ$ ) ( $\varepsilon = 2.445$  GeV) has been considered. The latter corresponds to experiment E89-033 performed at JLab [20, 33].

From inspection of Fig. 8 we may conclude the following:

- The largest differences are produced when comparing the two Weyl gauge prescriptions,

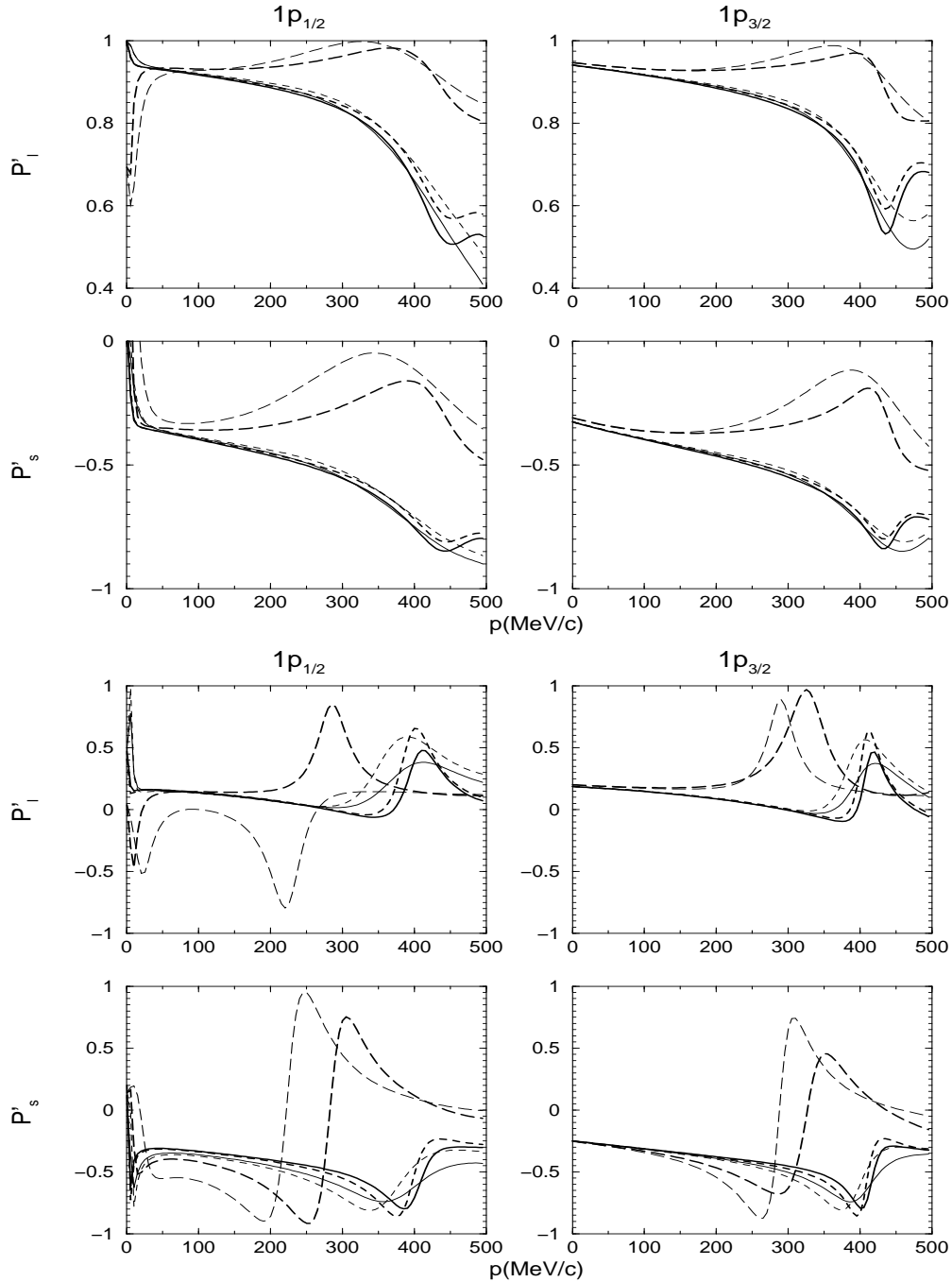


Figure 8: Transferred polarization asymmetries for longitudinal and sideways spin directions. The results are for kinematics 1 (see text). Top panels correspond to  $\theta_e = 150^\circ$  and bottom panels to  $\theta_e = 30^\circ$ . right-hand panels correspond to the  $p_{1/2}$  shell and left-hand panels to  $p_{3/2}$ . The labelling is the same as in Fig. 1.



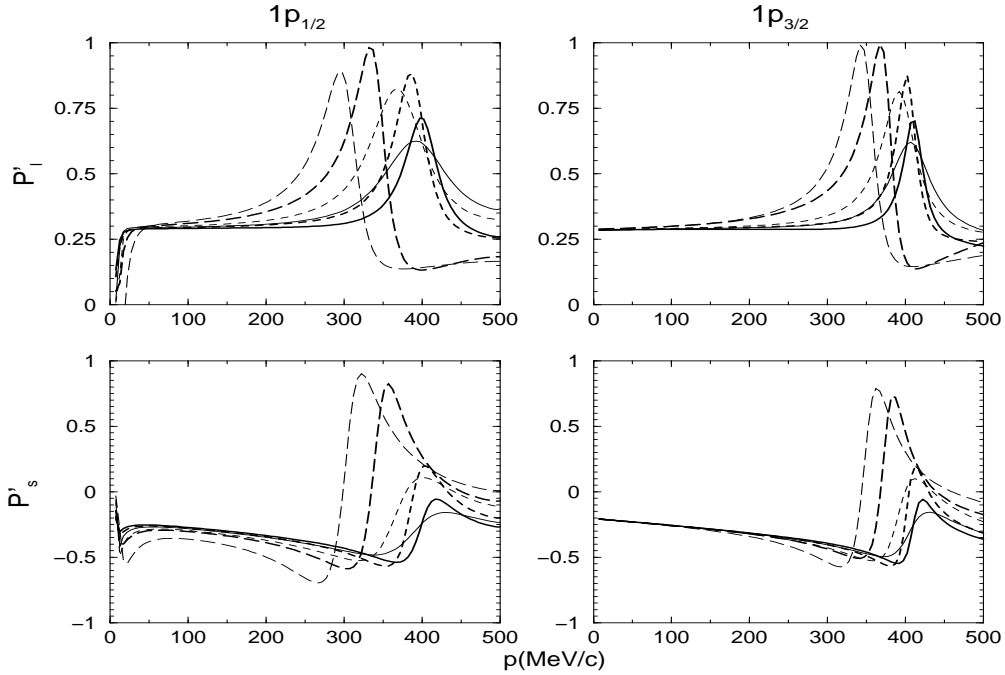


Figure 9: As for Fig. 8, but now for kinematics 2 and  $\theta_e = 23.4^\circ$

$CC1^{(3)}$  and  $CC2^{(3)}$ , with the other four prescriptions corresponding to the Coulomb and Landau gauges. Note, in particular, the behaviour of  $CC1^{(3)}$  for  $P'_l$  in the case of the  $p_{1/2}$  shell and forward electron scattering. On the other hand, the off-shell uncertainties are significantly reduced in the case of the Coulomb and Landau gauges based prescriptions.

- Off-shell uncertainties are enhanced for forward electron scattering. Contrary to backward scattering where the transverse responses dominate, for forward scattering angles all of the kinematical factors are of similar order and consequently, off-shell effects are maximized.
- Within the backward scattering situation (top panels), the two polarization asymmetries are very similar for the Coulomb and Landau gauges up to roughly  $p = 300$  MeV/c. For higher  $p$ -values, the four prescriptions start to deviate, although their differences are still relatively small.
- In the case of forward scattering (bottom panels), we should distinguish between  $P'_l$  and  $P'_s$ . In the former, Coulomb and Landau gauges with the two current choices give rise to almost identical results up to a missing momentum  $p = 300$  MeV/c. For  $p > 300$  MeV/c, the results deviate from each other, their difference being considerably larger than the one observed for backward scattering. For  $P'_s$  the differences amongst the four prescriptions associated with the Landau and Coulomb gauges start to be clearly visible at lower values of the missing momentum  $p$ .
- Finally, comparing the results for the  $p_{1/2}$  and  $p_{3/2}$  shells, we observe that the same

qualitative behaviour is obtained for all of the off-shell prescriptions, with the exception of  $CC1^{(3)}$  in  $P'_l$ . It is important to recall that the differences shown for both shells, which are larger for  $\theta_e = 30^\circ$ , come from the dynamical relativistic effects. Within PWIA, due to factorization, the polarization asymmetries only depend on the single-nucleon responses, i.e., they are not affected by the bound wave function selected. The different behaviour observed for both shells at very low  $p$ -values is directly connected to the quantum number  $\bar{\ell} = 0$  ( $\bar{\ell} = 2$ ) of the lower component in the  $p_{1/2}$  ( $p_{3/2}$ ) state (see [37] for details).

Transferred polarization asymmetries for kinematics 2 and  $\theta_e = 23.4^\circ$  are presented in Fig. 9. Some of the comments in the previous case can be also applied here; however, some significant differences are also seen. In particular, note that, although the Weyl gauge still gives rise to very different responses, the relative differences seen with the Coulomb and Landau gauges are not so significant. This is connected with the fact that at very forward angles the off-shell uncertainty spread introduced by the Landau and Coulomb gauges is already very wide. As in the previous case, off-shell ambiguities are maximized for  $p_{1/2}$ .

The role played by the dynamical enhancement of the lower components in the bound nucleon wave function is clearly seen in Fig. 10. Here the fully-relativistic RPWIA results (dashed lines) corresponding to the Coulomb gauge with the  $CC1$  and  $CC2$  choices of the current, are compared with the transferred polarizations obtained by projecting out the negative-energy components (dotted lines). As in previous figures, results for  $p_{1/2}$  (left-hand panels) and  $p_{3/2}$  (right-hand panels) are shown. Results correspond to kinematics 1, and forward ( $\theta_e = 30^\circ$ , bottom panels) and backward ( $\theta_e = 150^\circ$ , top panels) angles have been considered.

First, note the difference between the relativistic and projected results observed at very small missing momentum values for the  $p_{1/2}$  shell. As already mentioned (see [37] for details), this effect comes directly from the quantum number  $\bar{\ell}$  involved in the lower component of the bound state wave function ( $\bar{\ell} = 0$  for  $p_{1/2}$ ). Moreover, it is also important to point out that fully-relativistic and positive-energy projected results typically do not differ appreciably, especially for backward angles, for  $p$ -values up to  $\sim 300$  MeV/c, although at forward angles some noticeable spread occurs at low  $p$  for  $P'_s$ . For  $p > 300$  MeV/c relativistic and projected results start to deviate from each other. This general behaviour is what one expects because of the clear dominance of the positive-energy projection component of the momentum distribution in the region  $p \leq 300$  MeV/c [17, 37]. On the contrary, in the region of high missing momentum,  $p > 300$  MeV/c, the negative-energy components,  $N_{uv}(p)$ ,  $N_{vv}(p)$ , are similar to or even larger than  $N_{uu}(p)$ , and hence the effects of the dynamical enhancement of the lower components in the bound relativistic wave functions are clearly visible in the transfer polarization asymmetries.

From the results in Fig. 10 it is also clear that the dynamical effects are maximized in the forward electron scattering situation. Here the differences between fully-relativistic and projected results are significant even for low/medium  $p$ -values, in particular for the sideways transfer polarization,  $P'_s$ . As we know, the purely transverse responses dominate at backward angles, hence the most relevant contributions to the polarization asymmetries come from the transverse polarized responses  $R_l^{T'}$  and/or  $R_s^{T'}$  in the numerator, and from the unpolarized

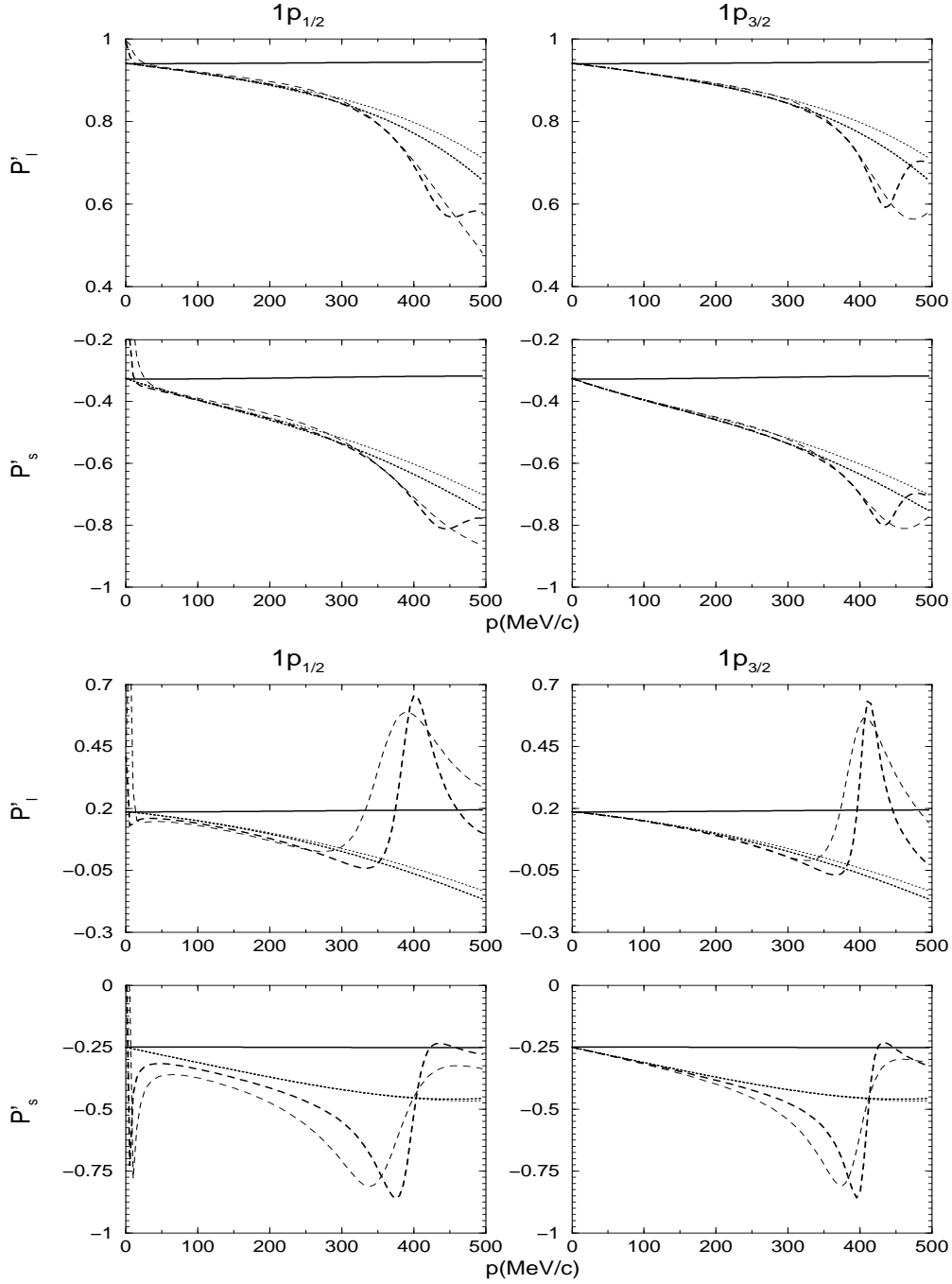


Figure 10: Transferred polarization asymmetries  $P'_l$  and  $P'_s$  for kinematics 1. Fully-relativistic results corresponding to the Coulomb gauge (dashed lines) are compared with their positive-energy projection contributions (dotted lines). Thin lines correspond to the  $CC1$  current operator and thick lines to  $CC2$ . We also show for comparison the static limit result (solid line).

$R^T$  response in the denominator of Eq. (17). From these three responses, only the small  $R_s^{T'}$  is particularly sensitive to the effect of the negative-energy components (see discussion in previous section). In contrast, at forward angles all of the kinematical factors that enter in the analysis of  $(\vec{e}, e'\vec{N})$  reactions are of similar order, and hence the contribution of these responses that are more sensitive to dynamical relativistic effects is maximized. Accordingly, the role played by the negative-energy components of the bound relativistic wave function is emphasized for transferred polarization asymmetries measured at forward angles. Although not shown for simplicity, these general comments also apply to the case of kinematics 2 and  $\theta_e = 23.4^\circ$ .

Finally, as it has been proven to be a suitable observable for getting information on nucleon properties in the nuclear medium [43], we present in Fig. 11 the ratio  $P'_s/P'_l$  (or the reverse in the case that  $P'_l$  goes through zero) for kinematics 1 and 2, respectively. As in previous figures, we present fully-relativistic results ( $CC1^{(0)}$  and  $CC2^{(0)}$ ) and their positive-energy projections, and we also show the results for the free-nucleon static limit as guidance. Following the general discussion already presented for the responses and polarization asymmetries, we find:

- Relativistic dynamical effects show up mainly for  $p > 300$  MeV/c, modifying completely the slowly-varying behaviour of the positive-energy results. Nevertheless, there exist already sizeable differences for low and moderate  $p$ -values for forward scattering angles.
- Forward scattering angles enhance the sensitivity to dynamical relativistic effects, particularly for the  $p_{1/2}$  shell, where relativistic effects show up clearly even at low/moderate values of the missing momentum. For the  $p_{3/2}$  shell these effects in the low and moderate  $p$  region are much less important.
- Relativistic and projected calculations deviate significantly from the free-nucleon static limit (solid line). At  $p = 100$  MeV/c the discrepancy is of the order of  $\sim 20$ – $50\%$  for kinematics 1 (the largest values corresponding to forward angle) and  $\sim 20$ – $35\%$  for kinematics 2.

To finish the discussion in this section, we show in Fig. 12 the transferred polarization asymmetries  $P'_l$ ,  $P'_s$  and ratio  $P'_l/P'_s$ , corresponding to parallel kinematics 4 and beam energy  $\varepsilon = 2.445$  GeV (we do not present results for kinematics 3, since in that case the outgoing nucleon kinetic energy selected only allows us to reach low/medium missing momentum values for which dynamical effects are expected to be less relevant). We observe that, in concert with the  $(q, \omega)$ -constant kinematics results, the highest differences between projected and fully relativistic results appear in the high- $p$  region, although also for low and moderate  $p$ -values one can find significant differences, mostly for the  $P'_l$  observable. This is connected with the fact that  $R_l^{T'}$  shows more sensitivity to dynamical relativistic effects than does  $R_s^{TL'}$  in parallel kinematics. Again, the differences for low and moderate  $p$ -values are much reduced in the  $p_{3/2}$  shell knockout case. Since the various off-shell prescriptions lead to different results for the two transferred polarization asymmetries and their ratio, clearly this impacts the determination of the single-nucleon properties in the nuclear medium; however,

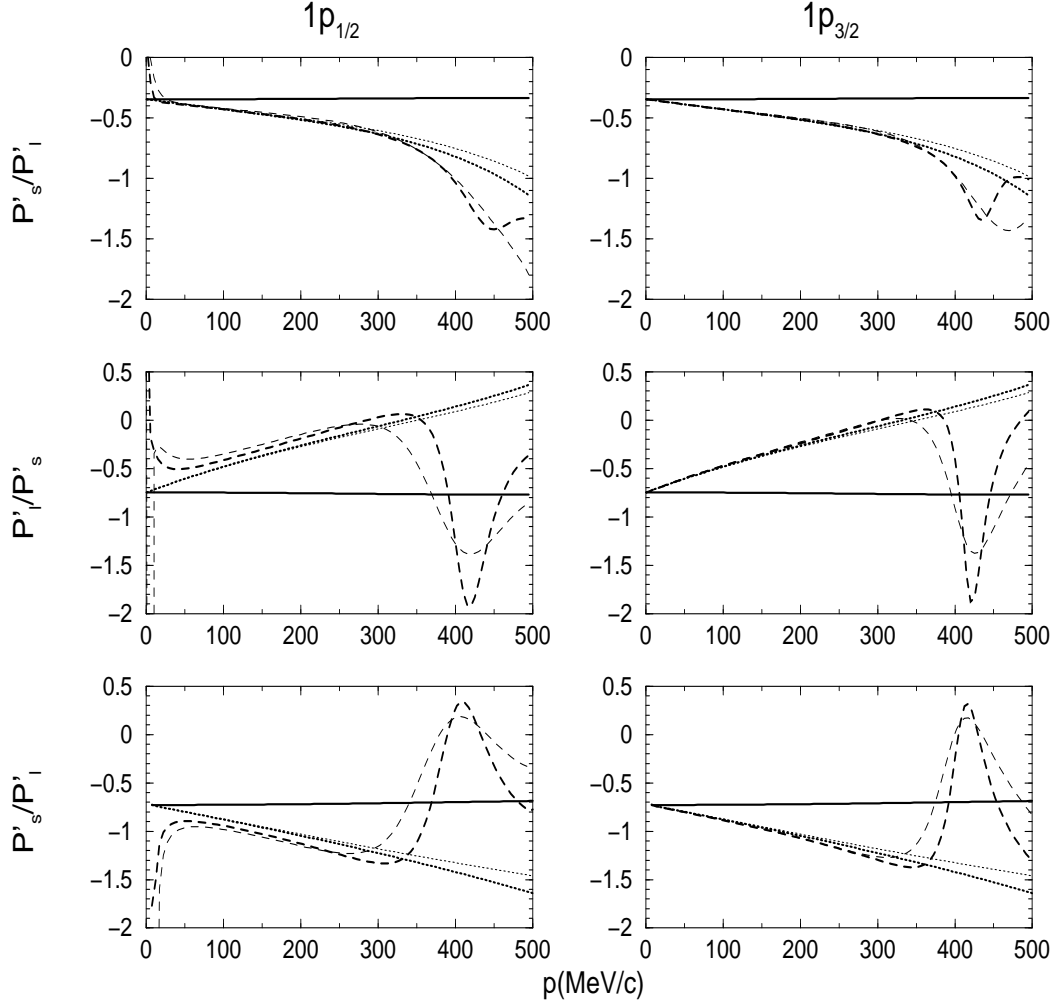


Figure 11: Ratios of polarization asymmetries for kinematics 1 and 2. Top (middle) panels correspond to  $\theta_e = 150^\circ$  ( $\theta_e = 30^\circ$ ) and kinematics 1, while bottom panels correspond to  $\theta_e = 23.4^\circ$  and kinematics 2. Results for the  $p_{1/2}$  (left-hand panels) and  $p_{3/2}$  (right-hand panels) shell are shown. The curves are labelled as in Fig. 10. For comparison we also present the static limit result (solid line).

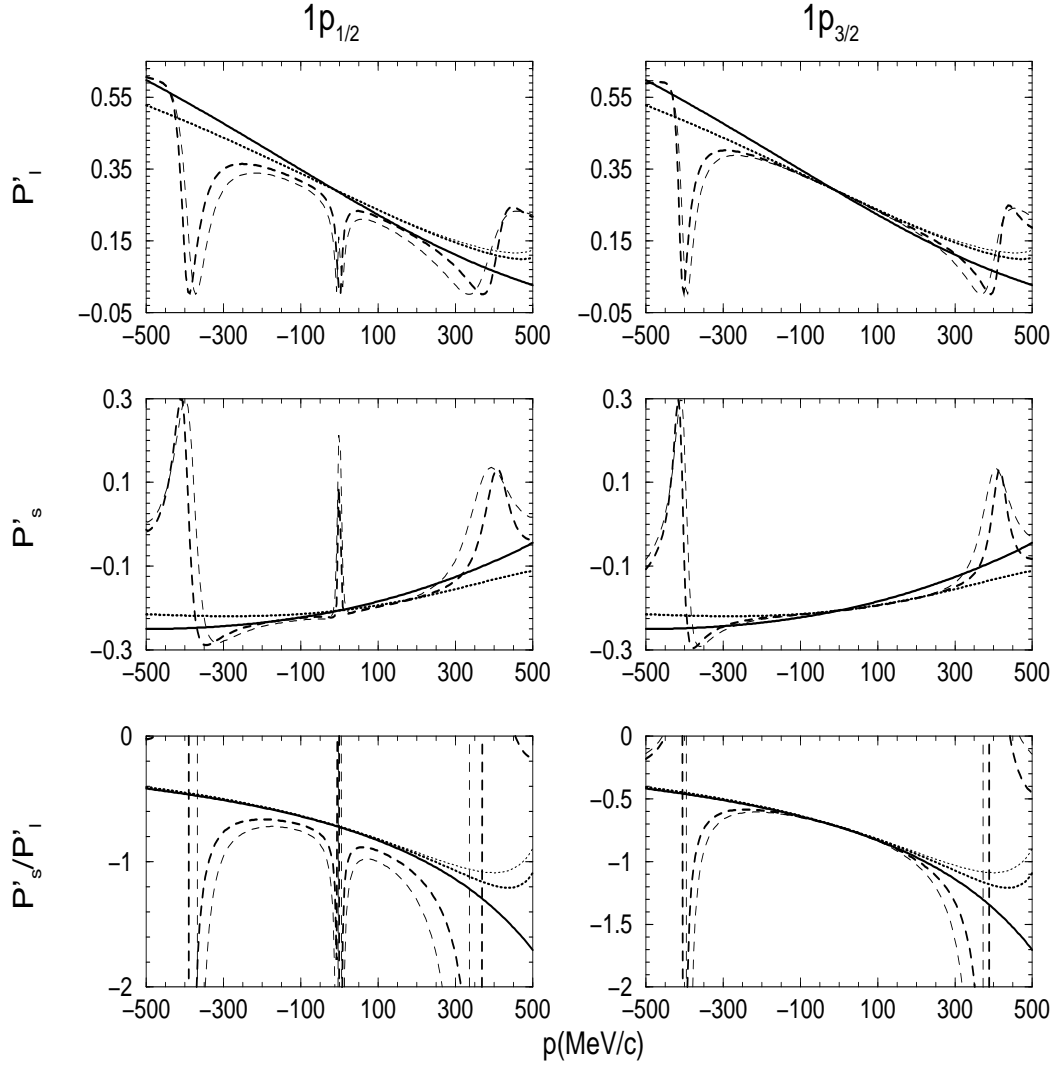


Figure 12: Transferred polarization asymmetries and ratio  $P'_l/P'_s$  for kinematics 4 and  $\varepsilon = 2.445$  GeV. Results for the  $p_{1/2}$  (left-hand panels) and  $p_{3/2}$  (right-hand panels) shell are shown. The curves are labelled as in Fig. 10 and Fig. 11.

without yet having all of the relativistic effects in hand — specifically, since we lack a treatment of the relativistic FSI problem within the same framework — it is premature to state the level of uncertainty that this entails. Upon completing the study discussed in the Introduction [32], the impact of all of the relativistic effects and the uncertainties they bring with them will be quantified.

## 4 Summary and conclusions

In this paper we have studied the  $A(\vec{e}, e'\vec{N})B$  reaction within RPWIA. Our aim has been to analyze dynamical relativistic effects associated with the bound nucleon wave function for polarized hadronic responses and transferred polarization asymmetries. Four different kinematical situations corresponding to  $(q, \omega)$ -constant (quasi-perpendicular) and parallel kinematics have been selected. In all cases results have been obtained for coplanar  $\phi = 0$  kinematics. Polarized observables have been evaluated for various choices of the current operator ( $CC1$  versus  $CC2$ ) and gauge (Coulomb, Landau and Weyl). As prototypical cases proton knock-out from the  $p_{1/2}$  and  $p_{3/2}$  shells in  $^{16}\text{O}$  has provided the focus. Note that this implies that the excitation energy  $\mathcal{E}$  has been taken to be small, corresponding to valence knock-out, and hence caution should be exercised in extending the conclusions presented here to the case of studies at large missing energy.

From the results and discussion presented in the previous sections, the following general conclusions can be drawn:

- The largest differences in the positive- and negative-energy projection components are produced by the prescriptions based on the Weyl gauge, particularly  $CC1^{(3)}$ . Moreover, off-shell uncertainties are much bigger for the negative-energy terms, whose relative contribution to the global responses is maximized by the  $CC1$  choice of the current.
- Within QEP kinematics, the responses  $R_s^{T'}$  and particularly  $R_l^{TL'}$  present the highest sensitivity to dynamical relativistic effects. Consequently, in light of the previous item, off-shell ambiguities are also bigger. On the contrary, the role of the negative-energy projections in the two remaining responses,  $R_l^{T'}$  and  $R_s^{TL'}$ , is almost negligible. Off-shell effects are also significantly reduced except for the Weyl gauge in  $R_s^{TL'}$ . These results also connect with the general study performed in [28] and also summarized above in Section 3.1, where the responses  $R_l^{T'}$  and  $R_s^{TL'}$  belong to class “0”, while  $R_s^{T'}$  and  $R_l^{TL'}$  are class “1” responses.
- Dynamical relativistic effects and off-shell ambiguity in the two purely transverse  $T'$ -responses are shown to diminish for higher  $q$ -values within the QEP. In the case of the two interference  $TL'$  responses and the prescriptions based on the Coulomb and Landau gauges, the effects introduced by the negative-energy projections and off-shell uncertainties change slightly as  $q$  varies within the QEP. Particularly interesting is the case of  $R_l^{TL'}$  and the  $CC1^{(0)}$  prescription for which dynamical relativistic effects do not depend on  $q$ .

- Within parallel kinematics, the two surviving responses,  $R_l^{T'}$  and  $R_s^{TL'}$ , are particularly sensitive to dynamical relativistic effects — much more than in the case of QEP kinematics. The spread of off-shell uncertainties is also wider in general. These results are directly connected with the fact that in parallel kinematics varying the missing momentum  $p$  means moving far away from the QEP, and consequently the role of negative-energy projections and off-shell effects are enhanced.
- Dynamical relativistic effects evaluated at  $p = \pm 100$  MeV/c (which corresponds approximately to the peaks of the responses), are shown to be larger for positive  $p$ -values than for negative  $p$ -values. This is so because positive  $p$ -values correspond to being further away from the QEP than the negative  $p$ -values with the same  $|p|$ . This seems to be correlated with the value of  $|y|/q$ . In fact, this also explains why the role of negative-energy projections, evaluated at the peaks of the responses, diminishes for larger outgoing nucleon momentum (kinematics 4), and why the behaviour shown for positive and negative  $p$ -values tends to be similar for increasing  $p_N$ .
- The influence of dynamical relativity and off-shell effects in the transferred polarization asymmetries is clearly maximized in the case of forward electron scattering. At high  $p$ -values the dynamical enhancement of the lower components in the bound nucleon wave function may modify completely the structure of the polarization asymmetries. In contrast, for  $p < 300$  MeV/c the negative-energy projections are in general well under control, and do not introduce significant effects, particularly for backward electron scattering.
- The dynamical relativistic results obtained for the ratio between longitudinal and side-ways transferred polarizations deviate significantly from the static limit approximation when using  $(q, \omega)$ -constant kinematics, even at low/medium  $p$ -values. Within parallel kinematics the discrepancies with the static limit diminish, especially in the case of the  $CC2$  current. However, even in this case, one should be very cautious before precise information on the in-medium nucleon form factors can be revealed from the analysis of  $(\vec{e}, e'\vec{N})$  reactions.
- Dynamical relativistic effects and off-shell uncertainties in the response functions are significantly reduced for a proton being knocked-out from the  $p_{3/2}$  shell which, having lower components of  $d$ -wave character rather than of  $s$ -wave character as in the  $p_{1/2}$  shell case, is natural. The transferred polarization asymmetries evaluated for both shells,  $p_{1/2}$  and  $p_{3/2}$ , in general display a similar structure, at high  $p$  showing an oscillatory behaviour that within RPWIA comes solely from the role played by the negative-energy components. This implies a crucial difference with respect to the standard PWIA and non-relativistic analyses.

Finally, although being aware of the significant modifications that FSI may introduce in the analysis, we are rather confident that the high sensitivity of polarization-related observables to negative-energy projections shown within RPWIA will probably also be maintained within more elaborated relativistic distorted-wave impulse approximation (RDWIA) calculations. Work along this line is presently in progress.



## Acknowledgements

This work was partially supported by funds provided by DGICYT (Spain) under Contracts Nos. PB/98-1111, PB/98-0676 and the Junta de Andalucía (Spain) and in part by the U.S. Department of Energy under Cooperative Research Agreement No. DE-FC02-94ER40818. M.C.M acknowledges support from a fellowship from the Fundación Cámara (University of Sevilla). J.A.C. also acknowledges financial support from MEC (Spain) for a sabbatical stay at MIT (PR2001-0185). The authors thank E. Moya, J.M. Udías and J.R. Vignote for their helpful comments.

## Appendix A

In this appendix we present the formalism needed to evaluate the positive- and negative-energy projection contributions to the hadronic tensor in the case of recoil nucleon polarization measurements.

The nucleon current matrix element in RPWIA is given by

$$\langle J^\mu \rangle \equiv \bar{u}(\mathbf{p}_N, s_N) \hat{J}^\mu \Psi_\kappa^m(\mathbf{p}) \quad (20)$$

with  $\Psi_\kappa^m(\mathbf{p})$  a relativistic bound nucleon wave function in momentum space. As already mentioned, this wave function has coupling to the negative-energy Dirac spinors  $v$ . Making use of the completeness relation for Dirac spinors or introducing positive- and negative-energy projector operators in Eq. (20), the nucleon current matrix element can be decomposed into two terms,  $\langle J^\mu \rangle = \langle J^\mu \rangle_u - \langle J^\mu \rangle_v$ , the former (latter) coming from the positive- (negative-) energy projector involving the Dirac spinors  $u(\mathbf{p}, s)$  ( $v(\mathbf{p}, s)$ ). These terms can be written in the form

$$\langle J^\mu \rangle_u = \sqrt{\frac{\bar{E} + M_N}{2M_N}} (-i)^\ell \alpha_\kappa(p) \sum_s [\bar{u}(\mathbf{p}_N, s_N) \hat{J}^\mu u(\mathbf{p}, s)] \langle s | \Phi_\kappa^m(\hat{\mathbf{p}}) \rangle \quad (21)$$

$$\langle J^\mu \rangle_v = -\sqrt{\frac{\bar{E} + M_N}{2M_N}} (-i)^\ell \beta_\kappa(p) \sum_s [\bar{u}(\mathbf{p}_N, s_N) \hat{J}^\mu v(\mathbf{p}, s)] \langle s | \Phi_{-\kappa}^m(\hat{\mathbf{p}}) \rangle, \quad (22)$$

where use has been made of the explicit expression of the relativistic bound nucleon wave function in momentum space as given in [17]. The term  $\langle s | \Phi_{\pm\kappa}^m(\hat{\mathbf{p}}) \rangle$  indicates spin projection of the bispinors  $\Phi_{\pm\kappa}^m$  on a spin state  $|\frac{1}{2}s\rangle$ , and the radial functions in momentum space  $\alpha_\kappa(p)$  and  $\beta_\kappa(p)$  were introduced in [17] and their explicit expressions are given in Eqs. (43,44).

Now we can proceed to evaluate the three contributions that enter in the hadronic tensor  $W^{\mu\nu}$  in Eq. (3).

- **Positive-energy projection tensor ( $W_P^{\mu\nu}$ ).**

$$W_P^{\mu\nu} = \frac{2}{2j+1} \sum_m \langle J^\mu \rangle_u^* \langle J^\nu \rangle_u. \quad (23)$$

Introducing the expression (21) one simply gets

$$W_P^{\mu\nu} = \frac{2}{2j+1} \frac{\bar{E} + M_N}{2M_N} |\alpha_\kappa(p)|^2 \sum_{ss'} \mathcal{W}_{ss'}^{\mu\nu} \sum_m \langle s | \Phi_\kappa^m \rangle^* \langle s' | \Phi_\kappa^m \rangle, \quad (24)$$

where the single-nucleon tensor  $\mathcal{W}_{ss'}^{\mu\nu}$  is defined as

$$\mathcal{W}_{ss'}^{\mu\nu} = \left[ \bar{u}(\mathbf{p}_N, s_N) \hat{J}^\mu u(\mathbf{p}, s) \right]^* \left[ \bar{u}(\mathbf{p}_N, s_N) \hat{J}^\nu u(\mathbf{p}, s') \right]. \quad (25)$$

Finally, using the relation

$$\sum_m \langle s | \Phi_\kappa^m \rangle^* \langle s' | \Phi_\kappa^m \rangle = \frac{2j+1}{8\pi} \delta_{ss'}, \quad (26)$$

the hadronic tensor contribution  $W_P^{\mu\nu}$  can be written in the form shown in Eq. (4).

- **Negative-energy projection tensor ( $W_N^{\mu\nu}$ ).**

Analogously to the previous case we have

$$W_N^{\mu\nu} = \frac{2}{2j+1} \sum_m \langle J^\mu \rangle_v^* \langle J^\nu \rangle_v \quad (27)$$

$$= \frac{2}{2j+1} \frac{\bar{E} + M_N}{2M_N} |\beta_\kappa(p)|^2 \sum_{ss'} \mathcal{Z}_{ss'}^{\mu\nu} \sum_m \langle s | \Phi_{-\kappa}^m \rangle^* \langle s' | \Phi_{-\kappa}^m \rangle, \quad (28)$$

with the single-tensor  $\mathcal{Z}_{ss'}^{\mu\nu}$  defined as

$$\mathcal{Z}_{ss'}^{\mu\nu} = \left[ \bar{u}(\mathbf{p}_N, s_N) \hat{J}^\mu v(\mathbf{p}, s) \right]^* \left[ \bar{u}(\mathbf{p}_N, s_N) \hat{J}^\nu v(\mathbf{p}, s') \right]. \quad (29)$$

Using again the relation (26), which means that only the spin-diagonal contributions survive, the hadronic tensor component  $W_N^{\mu\nu}$  factorizes into two terms as given in Eq. (5).

- **Crossed tensor ( $W_C^{\mu\nu}$ ).**

$$W_C^{\mu\nu} = -\frac{2}{2j+1} \sum_m \left[ \langle J^\mu \rangle_u^* \langle J^\nu \rangle_v + \langle J^\mu \rangle_v^* \langle J^\nu \rangle_u \right]. \quad (30)$$

Using the results shown in Eqs. (21,22) and taking into account that the radial functions  $\alpha_\kappa(p)$  and  $\beta_\kappa(p)$  in Eqs. (43,44) are both real, the hadronic crossed tensor can be written as

$$W_C^{\mu\nu} = \frac{\bar{E} + M_N}{8\pi M_N} \alpha_\kappa(p) \beta_\kappa(p) \sum_{ss'} \langle s' | \frac{\boldsymbol{\sigma} \cdot \mathbf{p}}{p} | s \rangle \left[ \mathcal{I}_{s's}^{\mu\nu} + (\mathcal{I}_{ss'}^{\nu\mu})^* \right], \quad (31)$$

where the single-nucleon tensor  $\mathcal{I}_{s's}^{\mu\nu}$  is given by

$$\mathcal{I}_{s's}^{\mu\nu} = \left[ \bar{u}(\mathbf{p}_N, s_N) \hat{J}^\mu u(\mathbf{p}, s) \right]^* \left[ \bar{u}(\mathbf{p}_N, s_N) \hat{J}^\nu v(\mathbf{p}, s') \right], \quad (32)$$

and the sum over  $m$  has been performed using the relation

$$\sum_m \langle s | \Phi_\kappa^m \rangle^* \langle s' | \Phi_{-\kappa}^m \rangle = -\frac{2j+1}{8\pi} \langle s' | \frac{\boldsymbol{\sigma} \cdot \mathbf{p}}{p} | s \rangle. \quad (33)$$

The single-nucleon tensors  $\mathcal{I}_{s's}^{\mu\nu}$ ,  $(\mathcal{I}_{ss'}^{\nu\mu})^*$  can be written using traces in the general form

$$\mathcal{I}_{s's}^{\mu\nu} = \frac{1}{16M_N^2} \text{Tr} \left[ \gamma_5 (\delta_{ss'} + \gamma_5 \mathcal{C}_{s's}') (\mathcal{P} + M_N) \bar{\mathcal{J}}^\mu (\mathcal{P}_N + M_N) (1 + \gamma_5 \mathcal{S}_N) J^\nu \right], \quad (34)$$

where we have introduced the pseudovector  $C_{ss'}^\mu = \langle \mathbf{p}, s' | \gamma^\mu \gamma^5 | \mathbf{p}, s \rangle$ , which reduces to the four-spin of the bound nucleon  $S_L^\mu$  in the diagonal case  $s = s'$ .

Splitting the tensor  $\mathcal{I}_{s's}^{\mu\nu}$  into its symmetric ( $\mathcal{S}$ ) and antisymmetric ( $\mathcal{A}$ ) terms this can be written in general

$$\mathcal{I}_{s's}^{\mu\nu} = \mathcal{S}_{s's}^{\mu\nu} + \mathcal{A}_{s's}^{\mu\nu}(S_N) + \delta_{ss'} [\mathcal{A}^{\mu\nu} + \mathcal{S}^{\mu\nu}(S_N)].$$

This means that the dependence on the recoil nucleon polarization is entirely contained in the antisymmetric spin non-diagonal and symmetric spin-diagonal terms. Carrying out the sum over  $s$  and  $s'$  indicated in Eq. (31), and taking into account the relation

$$\langle s | \boldsymbol{\sigma} \cdot \mathbf{p} | s \rangle = -\langle -s | \boldsymbol{\sigma} \cdot \mathbf{p} | -s \rangle, \quad (35)$$

it can easily be shown that the spin diagonal terms give no contribution. Hence the whole dependence on the outgoing nucleon four-spin  $S_N^\mu$  is contained in the surviving antisymmetric part of the tensor,  $\mathcal{A}_{s's}^{\mu\nu}$ . A similar analysis can be also applied to  $(\mathcal{I}_{ss'}^{\nu\mu})^*$ . Thus, we can write

$$\mathcal{I}_{s's}^{\mu\nu} + (\mathcal{I}_{ss'}^{\nu\mu})^* \equiv \mathcal{R}_{s's}^{\mu\nu} = (\mathcal{R}_{s's}^{\mu\nu})^{sym} + (\mathcal{R}_{s's}^{\mu\nu})^{ant} \quad (36)$$

with

$$(\mathcal{R}_{s's}^{\mu\nu})^{sym} = \frac{1}{8M_N} \text{Tr} \left[ \mathcal{C}_{s's'} \bar{\mathcal{J}}^\mu (\mathcal{P}_N + M_N) J^\nu \right] \quad (37)$$

$$(\mathcal{R}_{s's}^{\mu\nu})^{ant} = \frac{1}{8M_N} \text{Tr} \left[ \mathcal{C}_{s's'} \bar{\mathcal{J}}^\mu \gamma_5 \mathcal{S}_N (\mathcal{P}_N + M_N) J^\nu \right]. \quad (38)$$

The sum over  $s, s'$  can be explicitly performed, yielding

$$\sum_{ss'} \langle s' | \frac{\boldsymbol{\sigma} \cdot \mathbf{p}}{p} | s \rangle \mathcal{R}_{s's}^{\mu\nu} = (\mathcal{R}_{++}^{\mu\nu} - \mathcal{R}_{--}^{\mu\nu}) \cos \theta + (\mathcal{R}_{+-}^{\mu\nu} e^{-i\phi} + \mathcal{R}_{-+}^{\mu\nu} e^{i\phi}) \sin \theta, \quad (39)$$

with  $\theta, \phi$  the angles defining the direction of the bound nucleon momentum  $\mathbf{p}$ .

Finally, using the spin precession technique developed in [31], the different components of the spin-dependent tensor  $\mathcal{R}_{s's}^{\mu\nu}$  can be written in terms of a general spin-diagonal tensor  $\mathcal{R}^{\mu\nu}(S_L)$  in Eq. (11) whose spin four-vector  $S_L^\mu$  is quantized with respect to a generic direction defined by the angles  $(\theta_L, \phi_L)$  in the laboratory frame or  $(\theta_R, \phi_R)$  in the frame where the nucleon is at rest (see [31] for details). The final expression for the tensor  $\mathcal{N}^{\mu\nu}$  introduced in Eq. (6) is as given in Eq. (10). The components in the laboratory frame of the four-vector  $S_L^\mu$  needed to evaluate  $\mathcal{N}^{\mu\nu}$  are summarized in Table C.1 of [17].

## Momentum distribution components

The explicit expressions of the momentum distribution components  $N_{uu}(p)$ ,  $N_{vv}(P)$  and  $N_{uv}(P)$  introduced in Eqs. (4-6) are

$$N_{uu}(p) = \frac{\overline{E} + M_N}{8\pi M_N} |\alpha_\kappa(p)|^2 \quad (40)$$

$$N_{vv}(p) = \frac{\overline{E} + M_N}{8\pi M_N} |\beta_\kappa(p)|^2 \quad (41)$$

$$N_{uv}(p) = -\frac{\overline{E} + M_N}{4\pi M_N} \alpha_\kappa(p) \beta_\kappa(p), \quad (42)$$

with the functions  $\alpha_\kappa$  and  $\beta_\kappa$  given by

$$\alpha_\kappa(p) = g_\kappa(p) - \frac{p}{\overline{E} + M_N} S_\kappa f_\kappa(p) \quad (43)$$

$$\beta_\kappa(p) = \frac{p}{\overline{E} + M_N} g_\kappa(p) - S_\kappa f_\kappa(p), \quad (44)$$

and  $g_\kappa$ ,  $f_\kappa$  the Bessel transforms of the standard upper and lower radial functions of the bound nucleon wave function.

## Appendix B

In this appendix we present explicit expressions for the single-nucleon tensors  $\mathcal{W}^{\mu\nu}$ ,  $\mathcal{Z}^{\mu\nu}$  and  $\mathcal{R}^{\mu\nu}$  that enter in the analysis of  $A(\vec{e}, e'\vec{N})$  reactions within RPWIA. We show the results corresponding to the two current operators defined as *CC1* and *CC2* (see [28, 31, 36]). For simplicity we only show the expressions for the antisymmetric parts of the tensors which contain the entire dependence on the recoil nucleon polarization. The symmetric terms, giving rise to the unpolarized responses, are half the ones given in [17].

### • *CC1* current

$$\begin{aligned} \mathcal{W}_A^{\mu\nu} &= \frac{i}{2M_N^2} \left\{ M_N (F_1 + F_2)^2 \varepsilon^{\alpha\beta\mu\nu} S_{N_\alpha} \overline{Q}_\beta \right. \\ &\quad \left. + (F_1 + F_2) \frac{F_2}{2M_N} \left[ (\overline{P} + P_N)^\mu \varepsilon^{\alpha\beta\gamma\nu} - (\overline{P} + P_N)^\nu \varepsilon^{\alpha\beta\gamma\mu} \right] \overline{P}_\alpha P_{N_\beta} S_{N_\gamma} \right\} \quad (45) \end{aligned}$$

$$\begin{aligned} \mathcal{Z}_A^{\mu\nu} &= \frac{i}{2M_N^2} \left\{ M_N (F_1 + F_2)^2 \varepsilon^{\alpha\beta\mu\nu} (P_N + \overline{P})_\alpha S_{N_\beta} \right. \\ &\quad \left. + (F_1 + F_2) \frac{F_2}{2M_N} \left[ (\overline{P} + P_N)^\mu \varepsilon^{\alpha\beta\gamma\nu} - (\overline{P} + P_N)^\nu \varepsilon^{\alpha\beta\gamma\mu} \right] \overline{P}_\alpha P_{N_\beta} S_{N_\gamma} \right\} \quad (46) \end{aligned}$$

$$\begin{aligned}
\mathcal{R}_A^{\mu\nu}(S_L) &= \frac{i}{2M_N} \left\{ M_N (F_1 + F_2)^2 \varepsilon^{\alpha\beta\mu\nu} S_{L_\alpha} S_{N_\beta} \right. \\
&\quad \left. + (F_1 + F_2) \frac{F_2}{2M_N} [(\bar{P} + P_N)^\mu \varepsilon^{\alpha\beta\gamma\nu} - (\bar{P} + P_N)^\nu \varepsilon^{\alpha\beta\gamma\mu}] S_{L_\alpha} P_{N_\beta} S_{N_\gamma} \right\}
\end{aligned} \tag{47}$$

• *CC2 current*

$$\begin{aligned}
\mathcal{W}_A^{\mu\nu} &= \frac{i}{2M_N^2} \left\{ M_N F_1^2 \varepsilon^{\alpha\beta\mu\nu} S_{N_\alpha} \bar{Q}_\beta \right. \\
&\quad + \frac{F_1 F_2}{2M_N} [(Q^\mu \varepsilon^{\alpha\beta\gamma\nu} - Q^\nu \varepsilon^{\alpha\beta\gamma\mu}) S_{N_\alpha} P_{N_\beta} \bar{P}_\gamma \\
&\quad + 2\varepsilon^{\alpha\beta\mu\nu} (\bar{P} \cdot Q P_{N_\alpha} S_{N_\beta} - M_N^2 Q_\alpha S_{N_\beta})] \\
&\quad - \frac{F_2^2}{4M_N} [(Q^\mu \varepsilon^{\alpha\beta\gamma\nu} - Q^\nu \varepsilon^{\alpha\beta\gamma\mu}) S_{N_\alpha} (\bar{P} + P_N)_\beta Q_\gamma \\
&\quad \left. + \varepsilon^{\alpha\beta\mu\nu} (2\bar{P} \cdot Q S_{N_\alpha} Q_\beta + Q^2 (\bar{P} + P_N)_\alpha S_{N_\beta}) \right\}
\end{aligned} \tag{48}$$

$$\begin{aligned}
\mathcal{Z}_A^{\mu\nu} &= \frac{i}{2M_N^2} \left\{ M_N F_1^2 \varepsilon^{\alpha\beta\mu\nu} (\bar{P} + P_N)_\alpha S_{N_\beta} \right. \\
&\quad + \frac{F_1 F_2}{2M_N} [(Q^\mu \varepsilon^{\alpha\beta\gamma\nu} - Q^\nu \varepsilon^{\alpha\beta\gamma\mu}) S_{N_\alpha} P_{N_\beta} \bar{P}_\gamma \\
&\quad + 2\varepsilon^{\alpha\beta\mu\nu} (\bar{P} \cdot Q P_{N_\alpha} S_{N_\beta} - M_N^2 S_{N_\alpha} Q_\beta)] \\
&\quad + \frac{F_2^2}{4M_N} [(Q^\mu \varepsilon^{\alpha\beta\gamma\nu} - Q^\nu \varepsilon^{\alpha\beta\gamma\mu}) S_{N_\alpha} \bar{Q}_\beta Q_\gamma \\
&\quad \left. + \varepsilon^{\alpha\beta\mu\nu} (2\bar{P} \cdot Q Q_\alpha S_{N_\beta} + Q^2 \bar{Q}_\alpha S_{N_\beta}) \right\}
\end{aligned} \tag{49}$$

$$\begin{aligned}
\mathcal{R}_A^{\mu\nu}(S_L) &= \frac{i}{2M_N} \left\{ M_N F_1^2 \varepsilon^{\alpha\beta\mu\nu} S_{L_\alpha} S_{N_\beta} \right. \\
&\quad + \frac{F_1 F_2}{2M_N} [(P_N^\mu \varepsilon^{\alpha\beta\gamma\nu} - P_N^\nu \varepsilon^{\alpha\beta\gamma\mu}) S_{L_\alpha} S_{N_\beta} Q_\gamma \\
&\quad + \varepsilon^{\alpha\beta\mu\nu} (S_L \cdot Q P_{N_\alpha} S_{N_\beta} - P_N \cdot S_L S_{N_\alpha} Q_\beta - Q \cdot S_N S_{L_\alpha} P_{N_\beta})] \\
&\quad - \frac{F_2^2}{4M_N} [(Q^\mu \varepsilon^{\alpha\beta\gamma\nu} - Q^\nu \varepsilon^{\alpha\beta\gamma\mu}) S_{L_\alpha} S_{N_\beta} Q_\gamma \\
&\quad \left. + \varepsilon^{\alpha\beta\mu\nu} (2Q \cdot S_N S_{L_\alpha} Q_\beta - Q^2 S_{L_\alpha} S_{N_\beta}) \right\}
\end{aligned} \tag{50}$$

Finally, in Table 2 we show the components of the recoil nucleon spin 4-vector  $S_N^\mu$  in the laboratory frame along the three directions defined by the axes  $\mathbf{l}$ ,  $\mathbf{s}$  and  $\mathbf{n}$ .

Axis	$\mu = 0$	$\mu = 1$	$\mu = 2$	$\mu = 3$
$\mathbf{l}$	$\sqrt{\gamma_N^2 - 1}$	$\gamma_N \sin \theta_N$	0	$\gamma_N \cos \theta_N$
$\mathbf{s}$	0	$\cos \theta_N$	0	$-\sin \theta_N$
$\mathbf{n}$	0	0	1	0

Table 2: Components of the spin 4-vector  $S_N^\mu(\mathbf{l}, \mathbf{s}, \mathbf{n})$ . The notation  $\gamma_N \equiv E_N/M_N$  has been introduced.

## References

- [1] S. Boffi, C. Giusti, F.D. Pacati, M. Radici, “Electromagnetic Response of Atomic Nuclei”, (Oxford-Clarendon Press, 1996); Phys. Rep. **226** (1993).
- [2] J.J. Kelly, Adv. Nucl. Phys. **23** (1996) 77.
- [3] S. Frullani and J. Mougey, Adv. Nucl. Phys. **14** (1985).
- [4] A. Picklesimer and J.W. Van Orden, Phys. Rev. **C35** (1987) 266.
- [5] A. Picklesimer and J.W. Van Orden, Phys. Rev. **C40** (1989) 290.
- [6] M. Hedayati-Poor, J.I. Hohansson, H.S. Sherif, Phys. Rev. **C51** (1995) 2044; Nucl. Phys. **A593** (1995) 377.
- [7] J.J. Kelly, Phys. Rev. **C56** (1997) 2672; **59** (1999) 3256.
- [8] Y. Jin, D.S. Onley, Phys. Rev. **C50** (1994) 377.
- [9] J.M. Udías, P. Sarriguren, E. Moya de Guerra, E. Garrido, J.A. Caballero, Phys. Rev. **C48** (1993) 2731.
- [10] J.M. Udías, P. Sarriguren, E. Moya de Guerra, E. Garrido, J.A. Caballero, Phys. Rev. **C51** (1995) 3246.
- [11] J.M. Udías, P. Sarriguren, E. Moya de Guerra, J.A. Caballero, Phys. Rev. **C53** (1996) R1488.
- [12] J.M. Udías, J.A. Caballero, E. Moya de Guerra, J.E. Amaro, T.W. Donnelly, Phys. Rev. Lett. **83** (1999) 5451.
- [13] J.M. Udías, J.A. Caballero, E. Moya de Guerra, J.R. Vignote, A. Escuderos, Phys. Rev. **C64** (2001) 024614.
- [14] J.E. Amaro, J.A. Caballero, T.W. Donnelly, A.M. Lallena, E. Moya de Guerra, J.M. Udías, Nucl. Phys. **A 602** (1996) 263; **A 611** (1996) 163.
- [15] J.E. Amaro, M.B. Barbaro, J.A. Caballero, T.W. Donnelly, A. Molinari, Nucl. Phys. **A643** (1998) 349.

- [16] S. Jeschonnek, T.W. Donnelly, Phys. Rev. **C57** (1998) 2438.
- [17] J.A. Caballero, T.W. Donnelly, E. Moya de Guerra, J.M. Udías, Nucl. Phys. **A632** (1998) 323.
- [18] S. Gardner, J. Piekarewicz, Phys. Rev. **C50** (1994) 2822.
- [19] A.S. Raskin, T.W. Donnelly, Ann. Phys. **191** (1989) 78.
- [20] S. Malov et al., Phys. Rev. **C62** (2000) 057302. S. Malov, PhD thesis, New Brunswick, New Jersey, (1999), unpublished.
- [21] S. Dieterich et al., Phys. Lett. **B500** (2001) 47.
- [22] L. Eden et al., Phys. Rev. **C50** (1994) 1749.
- [23] B. Milbrath et al., Phys. Rev. Lett. **80** (1998) 452.
- [24] D. Eyl et al., Zeit. Phys. **A352** (1995) 211.
- [25] J.M. Udías, J.R. Vignote. Phys. Rev. **C62** (2000) 034302.
- [26] R.J. Woo et al., Phys. Rev. Lett. **80** (1998) 456.
- [27] J.J. Johansson, H.S. Sherif, Phys. Rev. **C59** (1999) 3481.
- [28] M.C. Martínez, J.A. Caballero, T.W. Donnelly, nucl-th/0201004, submitted to Nucl. Phys. **A**.
- [29] C. Giusti, F.D. Pacati, Nucl. Phys. **A504** (1989) 685.
- [30] J.D. Bjorken, S.D. Drell, Relativistic Quantum Mechanics, McGraw-Hill, New York, (1964).
- [31] J.A. Caballero, T.W. Donnelly, G.I. Poulis, Nucl. Phys. **A555** (1993) 709.
- [32] M.C. Martínez et al., in preparation (2002).
- [33] JLab Experiment E89-003, Spokespersons: W. Bertozzi, K. Fissum, A. Saha, L. Weinstein, unpublished.
- [34] JLab Experiment E89-033, Spokespersons: C.C. Chang, C. Glashauser, S. Nanda, P. Rutt, unpublished.
- [35] E. Garrido, J.A. Caballero, E. Moya de Guerra, P. Sarriguren, J.M. Udías, Nucl. Phys. **A584** (1995) 256.
- [36] T. de Forest, Nucl. Phys. **A392** (1983) 232.
- [37] J.A. Caballero, T.W. Donnelly, E. Moya de Guerra, J.M. Udías, Nucl. Phys. **A643** (1998) 189.

- [38] B.D. Serot, J.D. Walecka, *Adv. Nucl. Phys.* **16** (1986) 1.
- [39] C.J. Horowitz, B.D. Serot, *Phys. Lett.* **B86** (1979) 146; *Nucl. Phys.* **A368** (1981) 503.
- [40] C.J. Horowitz, D.P. Murdock, B.D. Serot, *Computational Nuclear Physics*, Springer, Berlin (1991).
- [41] M.M. Sharma, M.A. Nagarajan, P. Ring, *Phys. Lett.* **B312** (1993) 377.
- [42] G.A. Lalazissis, J. König, P. Ring, *Phys. Rev.* **C55** (1997) 540.
- [43] R.G. Arnold, C.E. Carlson, F. Gross, *Phys. Rev.* **C23** (1981) 363.